GEOLOGICA CARPATHICA, AUGUST 2018, 69, 4, 382–409 doi: 10.1515/geoca-2018-0023

Integrated biostratigraphical, sedimentological and provenance analyses with implications for lithostratigraphic ranking: the Miocene Komjatice depression of the Danube Basin

KATARÍNA ŠARINOVÁ[1,✉], SAMUEL RYBÁR[2], EVA HALÁSOVÁ[2], NATÁLIA HUDÁČKOVÁ[2], MICHAL JAMRICH[2], MARIANNA KOVÁČOVÁ[2] and MICHAL ŠUJAN[2]

[1]Department of Mineralogy and Petrology, Faculty of Natural Sciences, Comenius University in Bratislava, Mlynská dolina, Ilkovičova 6, 842 15 Bratislava, Slovakia; ✉sarinova@fns.uniba.sk
[2]Department of Geology and Paleontology, Faculty of Natural Sciences, Comenius University in Bratislava, Mlynská dolina, Ilkovičova 6, 842 15 Bratislava, Slovakia

(Manuscript received February 12, 2018; accepted in revised form May 31, 2018)

Abstract: The Komjatice depression, situated on the Danube Basin's northern margin, represents a sub-basin of the Neogene epicontinental Central Paratethys Sea and Lake Pannon. The paper provides an insight into the character of sediment provenance evolution by study of well cores (ZM-1, IV-1, MOJ-1, VR-1 wells). A modern combination of provenance, sedimentology and biostratigraphy together with the reported redefinition of Pannonian formations resulted in a new lithostratigraphy of the study area. Moreover, newly published volcanic rock age data were used for calibration of biostratigraphy. The overall age span of the sedimentary fill is occupied only by late Badenian–Sarmatian (Serravallian) to Pannonian (Tortonian–Messinian) strata: 1) the basal alluvial sediments of the newly defined Zlaté Moravce Formation; 2) late Badenian–Sarmatian (Serravalian) marine sediments of the Vráble-Pozba Fm., connected with tectonic opening of the depression; 3) Pannonian (Tortonian) coarse grained sediments of the Nemčiňany Fm. with an erosional base; 4) Pannonian (Tortonian–Messinian) predominantly fine-grained, basin floor to slope Ivanka Fm., sandy deltaic Beladice Fm. and predominantly muddy, alluvial Volkovce Fm. In the middle Miocene provenance is situated in Paleozoic sequences and Neogene volcanic rocks occurring currently in the NE. During the late Miocene, provenance is changed to the NNW (Tribeč Mts.), although the transport from the NE also remained.

Keywords: Neogene, Danube Basin, biostratigraphy, age calibration by volcanic rock provenance analysis, Zlaté Moravce Fm.

Introduction

The Komjatice depression forms a NE bay of the Danube Basin. It is bordered by the Tribeč Mts. in the N-NW and by Pohronský Inovec and Štiavnické vrchy Mts. in the E and SE (Fig. 1). The depression was opened by simple-shear mechanism (Hók et al. 2016) along the Mojmírovce fault zone and later influenced by thermal subsidence linked to cessation of volcanic activity (e.g., Kováč et al. 2018). The last stage is marked by marginal basin inversion (e.g., Šujan et al. 2016). The Pre-Cenozoic basement is built up by crystalline complexes of the Tatric and Veporic units and their cover and nappe units (Gaža & Beinhauerová 1976; Fusán et al. 1987a, b; Hók et al. 1999, 2016). The surrounding Pohronský Inovec and Štiavnické vrchy Mts. are formed by Neogene volcanic rocks (Fig. 1). Exploration wells, drilled in the 1960s and 1970s are essential for the geological research. Lithologies of the Neogene fill together with petrography of selected cores are described in the final drilling reports. These were summarized by Biela (1978a) and include biostratigraphic ranking based on the benthic foraminifera assemblages. This dataset was used for multiple studies which focused on subsidence history, depositional systems and tectono-sedimentary evolution of the Komjatice depression (e.g., Gaža & Beinhauerová 1976; Lankreijer et al. 1995; Hók et al. 1999, 2016; Kováč et al. 2006, 2010, 2011; Lénárt & Hók 2013). However, for biostratigraphic correlations planktonic foraminifera and calcareous nannofossil assemblages are the most suitable tools. In the studied area only the ŠVM-1 Tajná well was processed by modern methods (Kováč et al. 2006, 2008). Calcareous nannofossils were also analysed from a part of the ZM-1 well (Ozdínová 2012) and IV-1 well (Zahradníková et al. 2013). Sarmatian fish fauna was described from ŠVM-1 Tajná and JVM-2 by Chalupová (2006). In addition to biostratigraphic data, the first cosmogenic $^{10}Be/^{9}Be$ nuclides dating from VR-1 well, was published by Šujan et al. (2016). Recently new K/Ar and Rb/Sr age data from volcanic rocks, which form the eastern edge of the basin, have been published by Lexa & Pécskay (2010) and Chernyshev et al. (2013). These enabled indirect dating of volcanic material in the basin fill. From this point of view, the presented study is aimed at the reevaluation of stratigraphy and provenance analysis of the recently resampled deep wells.

Methodology

The analysis of the Komjatice depression was based on study of the available literature, including the original well protocols (Gaža 1968, 1970, 1975, 1977; Tanistrák 1969; Čermák 1972, 1976a, b, c; 1977a, b, c; Biela 1978a). The data was supplemented by investigation of well cores provided by Nafta petroleum company. Samples were taken from the Mojmírovce-1 (**MOJ-1**), Ivanka-1 (**IV-1**), Vráble-1 (**VR-1**) and Zlaté Moravce-1 (**ZM-1**) wells (Fig. 1, Table 1). For the purpose of the lithological and sedimentological description well core samples were cut in half perpendicularly to the bedding plane. Sedimentary textures and structures were documented mainly in the sense of Miall (2006), Nichols (2009) and Boggs (2006).

For petrography and provenance analyses conglomerate and sandstone samples were studied under a polarizing microscope. Abbreviations of minerals follow Withney & Evans

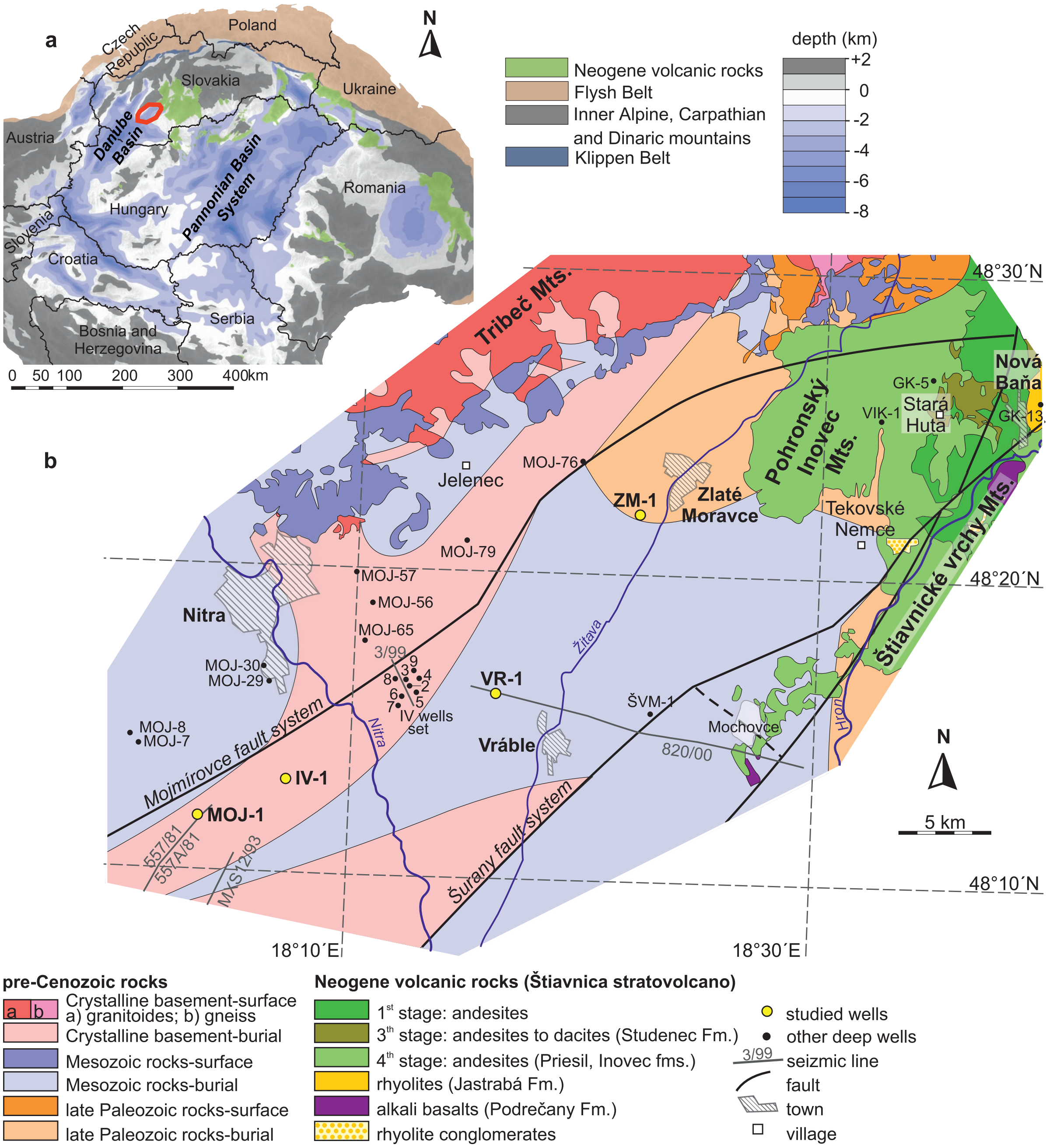

Fig. 1. Location map of the studied area: **a** — location in the Pannonian basin system; **b** — geological map (Káčer et al. 2013) with a view of the composition of the pre-Cenozoic basement (after Fusán et al. 1987b).

Table 1: Coordinates of the studied wells.

Well	WGS 84 decimal		WGS 84 degrees minutes seconds	
	x	y	Longitude	Latitude
ZM-1	18.37121	48.37382	18°22'16.35" E	48°22'25.74" N
VR-1	18.26955	48.27331	18°16'10.37" E	48°16'23.92" N
IV-1	18.13928	48.22312	18°08'21.42" E	48°13'23.24" N
MOJ-1	18.06612	48.19925	18°03'58.04" E	48°11'57.29" N

(2010). The heavy fraction was separated using heavy liquid from the 0.25–0.10 mm fraction (10 g) and studied under the binocular microscope. The specified heavy minerals were confirmed by EDAX analysis of microprobe CAMECA SX 100 (State Geological Institute of Dionýz Štúr). Selected heavy minerals and plagioclase were analysed by WDS analysis of microprobe CAMECA SX 100. Garnets were calculated to 8 cations and their molecule composition was calculated after Locock (2008). Together with the chemical composition of garnets mineral inclusions were observed. For provenance evaluation a modification of Suggate & Hall's (2014) diagram was used. Epidote/allanite were calculated to 8 cations, spinel to 3 cations and tourmaline to 31 anions. Feldspars were calculated to 8 anions. Bentonite was confirmed by X-ray diffraction on the Department of Mineralogy and Petrology, Comenius University in Bratislava.

Foraminifera have been obtained from 100 g of well core material, which was diluted by hydrogen peroxide and wet sieved (0.071 and 1 mm). The binocular stereoscopic microscope (Olympus SZ75) and the biological polarizing microscope were used for determination of foraminifera and the scanning electron microscope QUANTA FEG 250 was used for their imaging (Institute of Electrical Engineering, SAS). The obtained residua were split into approximately 300 specimens (if possible). Determination of foraminifers is based on Loeblich & Tappan (1992), Cicha et al. (1998), Łuczkowska (1974) and Holbourn et al. (2013). Due to the poor preservation of the foraminiferal tests some stay in open nomenclature.

Calcareous nannofossil smear slides were prepared by the standard method of decantation. The aim was to count 300 species from each sample (if possible). For microscopic evaluation Olympus BX 50, objective with 100× magnification and oil immersion was applied. Camera Olympus Infinity 2, with QuickPHOTO CAMERA 2.3 software was used to create photo documentation. Nannofossil determination was supported by MIKROTAX webpage and papers from fellow workers dealing with the Central Paratethys.

Standard palynological processing was used to extract the organic matter. The samples were treated with cold HCl (35 %) and HF (40 %) to remove carbonates and silica. The organic matter was separated from the undissolved particles using heavy liquid $ZnCl_2$ (density 2 g/cm^3). Samples were not oxidized at any stage. The palynological slides were prepared with glycerin, and alcohol as the mounting medium. Analyses were performed under the Leica light microscope combined with Nomarski interference contrast (NIC). Dinocyst taxonomy is in accordance with Lentin & Williams (1998) and biozonation according to Bakrač et al. (2012) and Magyar et al. (1999a, b).

Biostratigraphy

To confirm age assignment multiple samples were analysed for calcareous nannofossil, foraminiferal assemblages and palynomorphs including dinocysts (Figs. 2, 3; Suppl. 1; for the fauna list see Suppl. 2). Palynomorphs are generally well preserved, but the proportion of dinocysts and sporomorphs changes in the individual samples. Due to bad preservation a part of the studied fossils stays in the open nomenclature. Additionally, samples contained pieces of coal, palynomorphs, *Halicoryne* aff. *morelleti* algae, Porifera spicules, Ostracoda valves, Echinoid spines, Osteichthyes bones, teeth and scales. In the VR-1 well pyritized diatom valves are also present, whereas in the ZM-1 well *Limacina* sp. (*Spiratella*) remains were observed.

From the MOJ-1 well all studied samples were barren for nannofossils and dinocysts. In the foraminiferal assemblages the benthic species prevail (Suppl. 1). In the lower part (2100–2095 m) rare *Bogdanowiczia pocutica* (*Bathysiphon pocutica*) is present. A sample from a depth of 2010–2005 m contains rich *Halicoryne* aff. *morelleti* remains. In the following samples, the benthic *Elphidium* sp. div. and *Quinqueloculina–Miliolina* specimens are dominant. In the depth of 1848–1851 m *Elphidium hauerinum* and small echinate elphidia (*E. josephinum, E. aculeatum*) together with miliolids are present, but their ratio varies in the cores. In the depth of 1795–1798 m few elphidia are present. Planktic *Globigerinella obesa* and other fragments of the lower Miocene foraminifers, like *Lenticulina* sp. are found in the depth of 960–955 m.

From the IV-1 well, the first sample was taken from the muddy interval of a gravity flow (2316–2311 m). The nannofossil assemblage is dominated by *Braarudosphaera bigelowii* and *B. bigelowii parvula*, but the association does not contain biostratigraphical markers (Suppl. 1). Eocene and Oligocene redeposits are also observed. The following interval (2093–1956 m) is barren for dinocysts, with an exception of reworked ?*Deflandrea* sp. in the depth of 2090–2093 m. On the other hand, benthic foraminifera *Elphidium* sp. and species of *Quinqueloculina–Miliolina* genera are dominant. Elphidia prevail in the lower part; while in the depth of 2045–2040 m miliolids dominate. Foraminiferal assemblages include *Porosononion* sp., reworked foraminiferal tests of *Cassigerinella globulosa* and *Haplophragmoides* sp. *Halicoryne* aff. *morelleti* algae is also present (2045–2040 m). *Bolivina sarmatica* is found in the depth of 1956–1961 m. First occurrences of the dinocysts *Virgodinium* sp., *Spiniferites* sp. and freshwater algae *Spirogyra, Zygnema, Ovoidites* are identified in the depth of 1758–1763 m. Autochthonous Pannonian (Tortonian) nanofossil *Reticulofenestra tegulata* and dinocysts *Virgodinium asymmetricum, Spiniferites bentori pannonicus* are observed in the depth of 1603–1612 m. These dinocysts together with

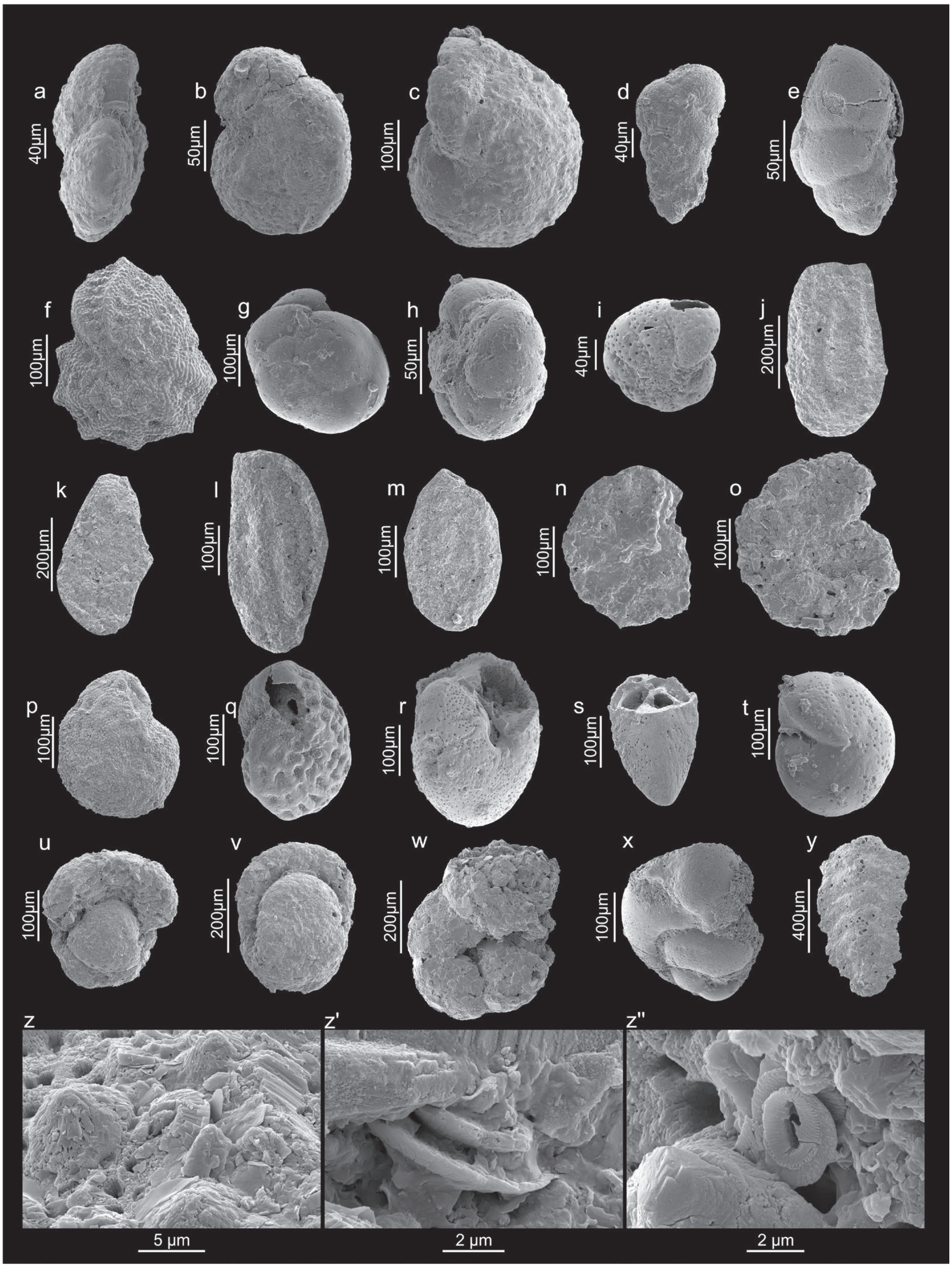

Fig. 2. Foraminifera and nannofossils in scanning electron microscope (c — core, b — core box): **a, b** — *Anomalinoides dividens* Łuczkowska, 1967; VR-1/c26, 1745–1750 m/b5; **c** — *Anomalinoides* cf. *dividens* Łuczkowska, 1967; VR-1/c26, 1745–1750 m/b5; **d** — *Bolivina sarmatica* Didkovski, 1959; VR-1/c26, 1745–1750 m/b5; **e** — *Protoglobobulimina pupoides* (d'Orbigny, 1846); VR-1/c26, 1745–1750 m/b5; **f** — *Elphidium josephinum* (d'Orbigny, 1846); VR-1/c22, 1550–1555 m/b3; **g, h** — *Ammonia tepida* (Cushman, 1926); VR-1/c19, 1405–1409 m/b5-4; **i** — *Porosononion granosum* (d'Orbigny, 1846); VR-1/c15, 1203–1208 m/b5; **j** — *Miliammina subvelatina* Venglinskyi, 1975; VR-1/c14, 1149–1154 m/b2; **k** — *Hyperammina* cf. *praelonga* Venglinskyi, 1970; VR-1/c14, 1149–1154 m/b2; **l** — *Miliammina subvelatina* Venglinskyi, 1975, VR-1/c14, 1149–1154 m/b2; **m** — *Miliammina fusca* (Brady, 1870); VR-1/c14, 1149–1154 m/b2; **n, o** — ?*Trochammina kibleri* Venglinskyi, 1961; VR-1/c14, 1149–1154 m/b2; **p, q** — *Elphidium hauerinum* (d'Orbigny, 1846); VR-1/c14, 1149–1154 m/b3; **r** — *Melonis pompilioides* (Fichtel & Moll, 1798); ZM-1/c16, 1253–1258 m/b2; **s** — *Bolivina dilatata* Reuss, 1850; ZM-1/c18, 1346–1351 m/b2; **t** — *Heterolepa dutemplei* (d'Orbigny, 1846); ZM-1/c18, 1346–1351 m/b2; **u** — *Budashevaella multicamerata* (Voloshinova, 1961); ZM-1/c18, 1346–1351 m/b4; **v** — *Alveolophragmium* sp., ZM-1/c18, 1346–1351 m/b4; **w** — *Haplophragmoides* cf. *fragile* Höglund, 1947; ZM-1/c18, 1346–1351 m/b4; **x** — *Uvigerina* sp. pyrite mold, ZM-1/c18, 1346–1351 m/b4; **y** — *Spirorutilus carinatus* (d'Orbigny, 1846); ZM-1/c18, 1346–1351 m/b4; **z, z'** — *Coccolithus pelagicus* (Wallich, 1877) Schiller, 1930, ZM-1/c18, 1346–1351 m/b2; **z"** — *Helicosphaera walbersdorfensis* Muller, 1974; ZM-1/c18, 1346–1351 m/b2.

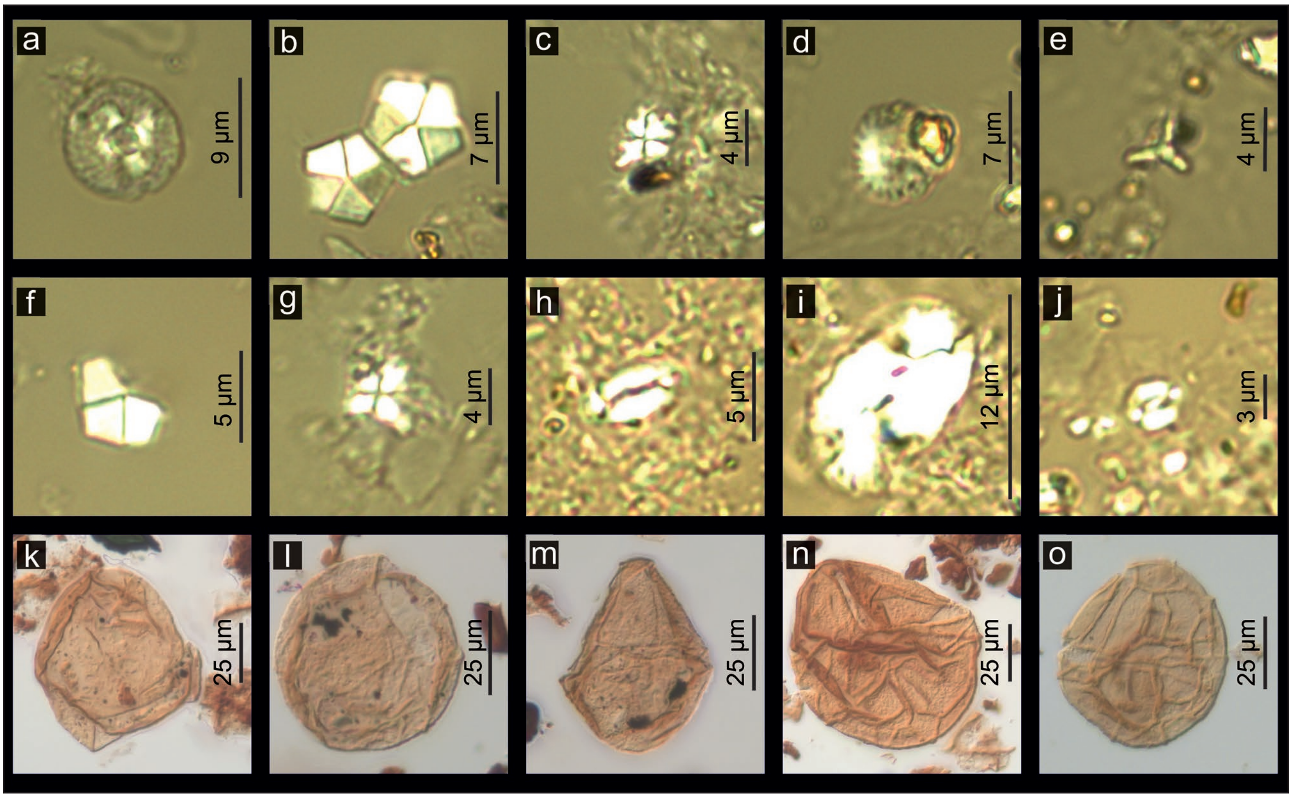

Fig. 3. Nannofossils and dinoflagellata in light microscope. **a** — *Calcidiscus tropicus* (Kamptner, 1955) Varol, 1989 *sensu* Gartner, 1992; VR1/c16, 1250–1255 m; **b** — *Braarudospahera bigelowii parvula* Stradner, 1960; VR1/c15, 1203–1208 m; **c** — *Sphenolithus abies* Deflandre in Deflandre & Fert, 1954; VR1/c15, 1203–1208 m; **d** — *Calcidiscus pataecus* (Gartner, 1967) de Kaenel & Villa, 1996; VR1/c14, 1149–1154 m; **e** — *Isolithus semenenko* Luljeva, 1989; VR1/c14, 1149–1154 m; **f** — *Braarudosphaera bigelowii parvula* Stradner, 1960; ZM1/c16, 1253–1258 m; **g** — *Sphenolithus abies* Deflandre in Deflandre & Fert, 1954; ZM1/c16, 1253–1258 m; **h** — *Helicosphaera walbersdorfensis* Müller, 1974; ZM1/c15, 1201–1206 m; **i** — *Helicosphaera wallichii* (Lohmann, 1902) Okada & McIntyre, 1977; ZM1/c15, 1201–1206 m; **j** — *Reticulofenestra tegulata* (Bóna & Gál, 1985; Ćorić & Gross, 2004); ZM1/c11/1005–1010 m; **k** — *Chytroeisphaeridia cariacoensis* Wall, 1967; VR1/c11, 1000–1005 m; **l** — *Chytroeisphaeridia cariacoensis* Wall, 1967; VR1/c11, 1000–1005 m; **m** — *Virgodinium asymmetricum* Sütő-Szentai, 2010; VR1/c11, 1000–1005 m; **n** — *Impagidinium spongianum* Sütő-Szentai, 1985; VR1/c7, 802–807 m; **o** — *Impagidinium spongianum* Sütő-Szentai, 1985; VR1/c5, 703–707 m.

Impagidinium spongianum, Achomosphaera sp., *Pontiadinium pecsvaradensis* are present in the depth of 1506–1509 m.

In the VR-1 well benthic foraminiferal species prevail. The planktonic species are possibly reworked from the lower Miocene sediments (*Globigerina* sp. div; *G. concinna, Cassigerinella globulosa*, *Trilobatus trilobus*, and *Globigerinella obesa*) or even Eocene–Oligocene such as *Chiloguembelina cubensis* (1750–1304 m). The lower part of the Neogene fill is barren for index species (Suppl. 1). In the depth interval of 1801–1804 m one specimen of the dinocyst ?*Cleistosphaeridinium placacanthum* is found together with an abundant nannofossil assemblage with poorly preserved *Helicosphaera* cf. *wallichii*, *H. walbersdorfensis, Reticulofenestra pseudoumbilicus*, *Calcidiscus* sp. and allochthonous Cretaceous, Paleogene and early Badenian nannofossils (1804–1745 m). The foraminifer *Anomalinoides dividens* (acme) is recognized in the depth of 1745–1750 m. The depth interval from 1555 to 1203 m contains *Porosononion granosum, Ammonia* sp., *Elphidium* sp. (from 1510 m) and *Nonion* sp. (from 1455 m) (Fig. 2) together with *Cycloforina badenensis* in the lower part of this interval. Nannofossil assemblages in this depth (1750–1203 m) contain *Calcidiscus tropicus*, *C. pataecus* (Fig. 3), *Calcidiscus macintyrei* and others (Suppl. 1). Moreover sphenoliths of Paleogene age are present. In the depth of 1203–1208 m only well preserved terrestrial palynomorphs without dinoflagellates are observed. The following interval (depth 1149–1154 m) contains the foraminifera ?*Trochammina kibleri* (Fig. 2) and *Dogielina* sp. together with the acme event of *Isolithus semenenko* (Fig. 3). The foraminifera *Miliammina* sp. (Fig. 2) and *Dogielina* sp. together with *Isolithus semenenko* are also found in the depth of 1103–1108 m. In the following part, well diversified dinoflagellata are observed (1000–1108 m), while the depth between 950–955 m is characterized by absence of dinocysts, presence of terrestrial and freshwater elements (*Zygnema, Nuphar*), as well as reworked dinoflagellata (*Deflandrea*). The higher depth intervals contain *Virgodinium asymmetricum, V. transformis, Impagidinium spongianum, Spiniferites bentori pannonicus, S. bentori* *oblongus, Achomosphaera* sp., *Chytroeisphaeridia cariacoensis* (750–755 m); *Virgodinium asymmetricum, V. transformis, Pontiadinium pecsvaradensis, Impagidinium spongianum, Chytroeisphaeridia cariacoensis* (703–707 m) and *V. asymmetricum, P. pecsvaradensis* (603–607 m).

The lower part of the ZM-1 well is barren for index fossils. Only poor nannofossils are observed in the depth of 1555–1551 m (Suppl. 1). However, the following well cores contained poor and badly preserved foraminiferal assemblages. In the depth of 1405–1410 m possible (? undetermined) agglutinated foraminifera or testaceans, glyptostrobus seeds and cone parts are present. In the depth of 1346–1351 m, remains of *Nonion communis, Bulimina elongata, Haplophragmoides* sp., *Reticulophragmium* sp., *Bathysiphon* sp., *Uvigerina semiornata, Haplophragmoides wilsoni, Spirorutilus carinatus* (Fig. 2), together with dinocysts *Melitasphaeridium choanophorum*, *Cleistosphaeridinium placacanthum* and Cretaceous reworked foraminifers are present. For the depth of 1253–1258 m an abundant and diversified foraminiferal association is typical, but tests are fragmented and show signs of dissolution. The most abundant are *Bolivina dilatata maxima*, *Melonis pompilioides* (Fig. 2), *Angulogerina angulosa, Valvulineria complanata,* bryozoans and ostracoda valves. Nannofossil assemblages from this interval (1351–1201 m) contain *Braarudosphaera bigelowii bigelowii*, *Calcidiscus leptoporus*, *C. premacintyrei*, *C. macintyrei*, *C. tropicus*, *Helicosphaera walbersdorfensis*, *H. wallichii*, *Holodiscolithus macroporus*, *Reticulofenestra pseudoumbilicus*, *Sphenolithus abies*, *Umbilicosphaera rotula* (Fig. 3). The association in the depth of 1046–1051 m is highly dominated by the foraminifer *Bolivina dilatata maxima* (Fig. 2) and by poorly preserved *Calcidiscus* spp. nannofossils. *Reticulofenestra tegulata* acme (Fig. 3) is present in the depth of 1010–1005 m. *Spiniferites bentori pannonicus* (653–658 m) is also present in the depth of 599–604 m together with *Impagidinium spongianum. I. spongianum* and *Spirogyra* are found in the depth of 551–556 m.

Lithology and composition of Neogene fill

MOJ-1 well

The leucocratic granite in the depth of 2099–2129 m (Figs. 4, 5) is composed of Qz, Pl, Mc, Or, Ms and Zrn. Fissures in the granites are filled by secondary carbonates.

The basal part of the Neogene fill (2099–1790 m; Figs. 4, 5) is composed of massive, lithic, medium-grained sandstones to fine-grained conglomerates, which interfinger with laminated mudstones. Mudstones include sporadic, lenticular sandy ripples. In the depth of 1790–1640 m the character of the sedimentary fill changes (Fig. 5). According to well logs and description of cuttings (Tanistrák 1969) three major gravelly–sandstone intervals divided by muddy horizons were recognized. Fine-grained conglomerates and sandstones are poorly sorted and display intervals with normal gradation and rare mud intraclasts (max. 3 cm). Normally graded conglomerates and sandstones are followed by ripples forming flaser structure. The top of the ripples is coated by carbonized plant fragments (Fig. 5). The sedimentary interval between 1640–980 m displays a heterolithic character but sandstones dominate. The mudstones are laminated; commonly bioturbated and ripples form flaser to wavy bedding. They rarely include articulated shells of *Congeria czizeki* (1253–1261 m) and fragmented limnocardid bivalves (1000–1005 m; Fig. 5). In the sandstones normal gradation and lamination is highlighted by carbonized plant fragments. In the lower part (1600–1300 m) the sandstones are better sorted and grains are more rounded. The sorting and roundness decreases again in the depth range from 1300 to 1000 m. The sediment in the interval of 980–395 m is characterized by alteration of sandstones and mudstones with red mottles, but sandstones are slightly more abundant. In the well cores we recognize rip-up clasts, rhizoids and bioturbations (Fig. 5).

The sandstones and conglomerates are composed of monocrystalline quartz (Qz), epiclastic carbonates, Qz+mica schists, granitoid, polycrystalline Qz, microcline (Mc), orthoclase (Or), plagioclase (Pl), rare muscovite (Ms), chlorite (Chl), garnet (Grt), zircon (Zrn), turmaline (Tur) and rutile (Rt). In the basal part, carbonate overgrowth, foraminifera test, Glt and framboidal Py were observed. In addition, carbonate fissures which cut mineral grains, were present (depth 2050 m; Fig. 6), which indicates disintegration after lithification. The mineral maturity (amount of monocrystalline Qz) increases upwards. The most pronounced change in the composition is the presence of intensively coloured Chl and Bt at a depth above 980 m. The amount of carbonate cement decreased upward, however the sample from the depth of 1397 m is heavily cemented with several generations of carbonate including poikilitic cement and carbonate clasts covered by iron oxides. A sample from the depth of 705 m also contains poikilitic cement.

Heavy mineral associations were analysed from four sandy samples (depth 1760 m, 2×1000 m and 550 m). Their composition is the same for all samples. Among transparent heavy minerals Grt (20–44 %) and Tur (4–26 %) dominate. Small amounts of Zrn, Ap, Rt, staurolite (St) and sillimanite (Sil< 2 %) occur. The association is completed by Ilm (7–17 %), Glt (up to 0.5 %) and framboidal pyrite (Py) together with limonite minerals (21–60 %). Samples from 1000 m rarely contain epidote (Ep) and magnesio-ferri-hornblende. Associations from depths of 1000 and 1760 m also show a strong leucoxenization, manifested by the presence of ferric oxide/hydroxide coating mineral grains (mainly carbonates). Framboidal pyrite is oxidized. In the depth of 550 m oxidation is minimal and moreover crystalline pyrite was also documented. Additionally, zonal Tur with a schorl core and dravite rim is found. Other Tur of dravite composition did not show significant zoning.

IV-1 well

The dark-grey to grey-green basement rocks show an oriented porphyroclastic–mylonite texture (2390 m; Figs. 7, 8).

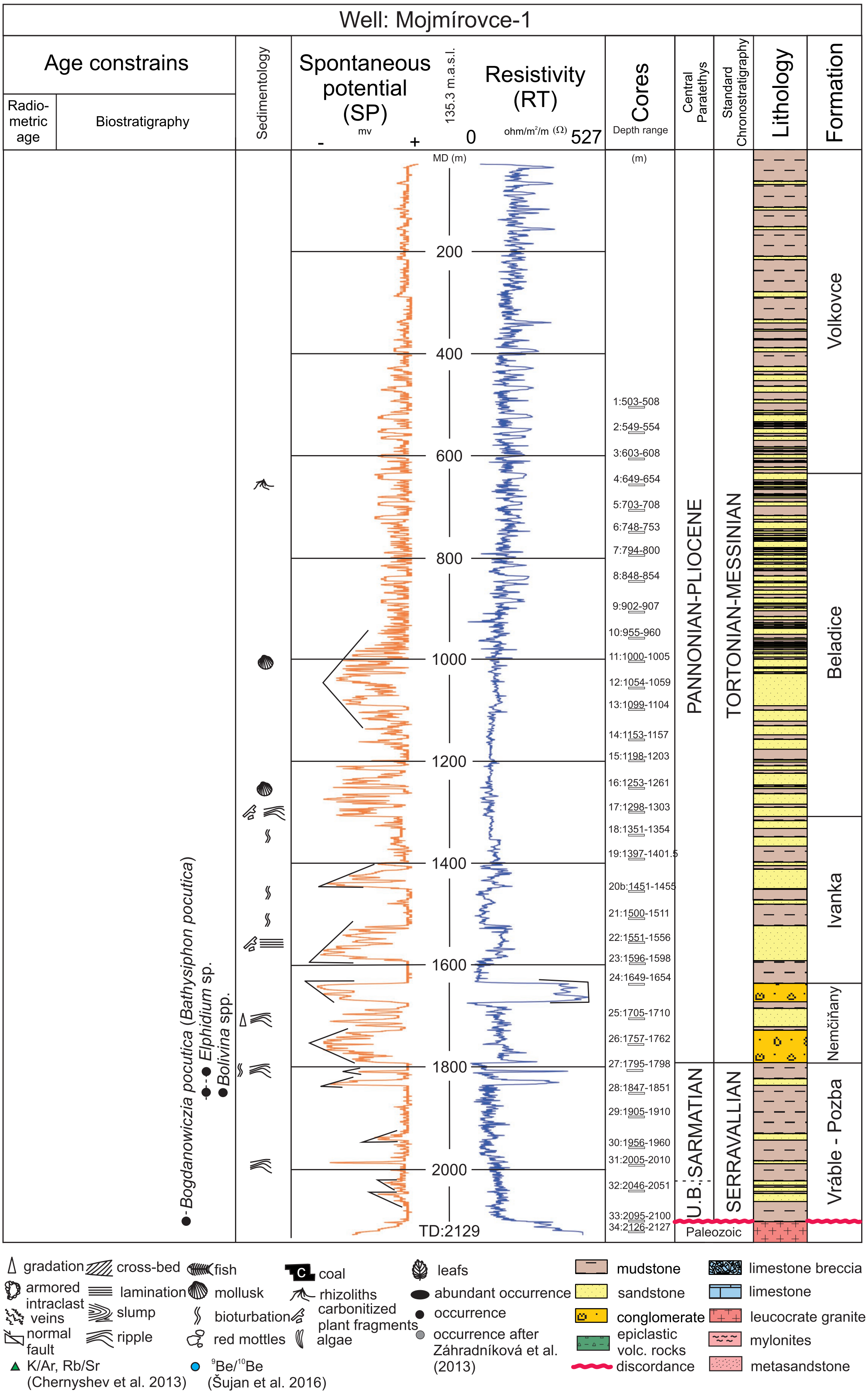

Fig. 4. MOJ-1 well table.

Fig. 5. MOJ-1 well core samples (scale bar= 1 cm, arrow pointing upwards, dot=bedding plane): **a** — leucocratic granite; MOJ-1/c33, 2095–2100 m/b2; **b** — heterolithic sediment with lenticular sandy ripples; MOJ-1/c31, 2005–2010 m/b2; **c** — heterolithic sediment with sandy ripples; MOJ-1/c27, 1795–1798,5 m/b5; **d** — poorly sorted conglomerate with poorly rounded clasts reach 2–3 mm in diameter; MOJ-1/c27, 1795–1798,5 m/b5; **e** — fluent transition from normally graded sandstone through laminated sandstone to sandy ripples which are draped by carbonized plant fragments (gravity flow sediment); MOJ-1/c25, 1705–1710 m; **f** — the same as e, but with an erosive contact on the top; MOJ-1/c25, 1705–1710 m/b1; **g** — normally graded coarse-grained sandstone to conglomerate (max. 2–5 mm diameter) with mudstone intraclasts; MOJ-1/c25, 1705–1710 m/b4; **h** — laminated, fine-grained sandstone. Laminae are formed by carbonized plant fragments; MOJ-1/c22, 1551–1556 m/b1; **i** — bioturbated mudstone with sporadic sandy laminae; MOJ-1/c18, 1351–1354 m; **j** — medium-grained sandstone ripples forming flaser bedding; MOJ-1/c17, 1298–1303 m/b4; **k** — *Congeria* cf. *czjzeki* Hörnes. MOJ-1/c16,1253–1261 m/b6; **l** — indistinctly bioturbated mudstone; MOJ-1/c16, 1253–1261 m/b5; **m** — massive mudstone witch carbonized plant fragments; MOJ-1/c13, 1099–1104 m/b1; **n** — massive sandstone; MOJ-1/c12, 1054–1059 m/b2; **o** — Cardiidae indet.; MOJ-1/c11, 1000–1005 m/b4; **p** — massive, medium-grained sandstone; MOJ-1/c11, 1000–1005 m/b2; **r** — mudstone with sandy concretions, red mottles and rhizoids; MOJ-1/c10, 955–960 m/b4; **s** — massive, medium-grained sandstone with a reddish mudstone intraclast; MOJ-1/c5, 703–708 m/b1; **t** — mudstone with red mottles, and rhizoids; MOJ-1/c4, 649–654 m/b2; **u** — massive medium-grained sandstone; MOJ-1/c2, 549–554 m/b2.

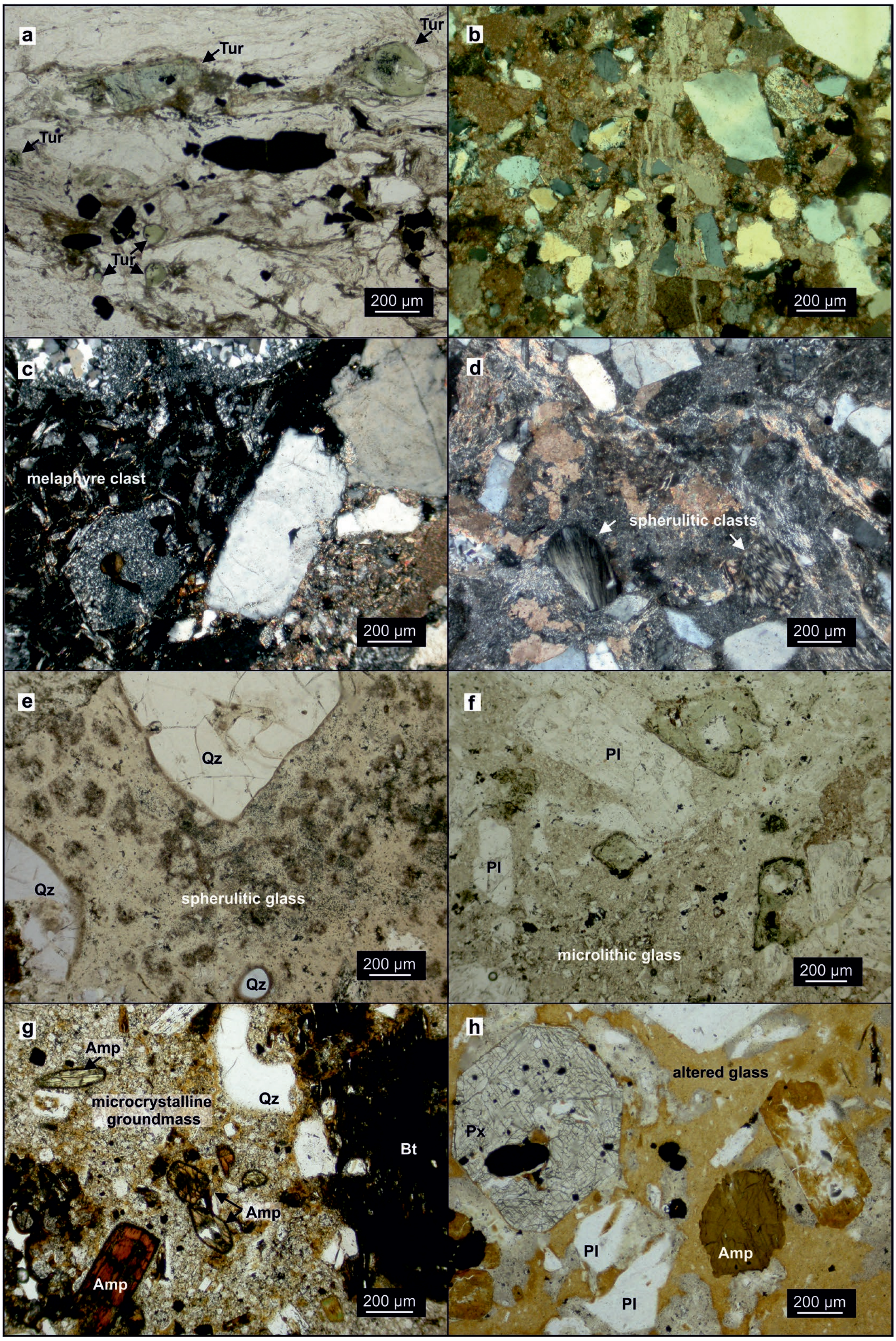

Fig. 6. Thin section: **a** — mylonite with idiomorphic tourmaline, plane-polarized light (PPL), IV-1/c21, 2355–2358 m/b3; **b** — detrital grains cut by calcite veins, sandstone, crossed polars (CP), MOJ-1/c32, 2046–2051 m; **c** — melaphyre clast in conglomerate (CP), IV/c20, 2311–2316 m/b2; **d** — spherulite clasts in fine-grained conglomerate (CP), VR-1/c35, 2202–2207 m/b1; **e** — spherulitic rhyolite clast from conglomerate (PPL), VR-1/c33, 2104–2109 m; **f** — andesite clast from conglomerate (PPL), VR-1/c32, 2054–2059 m/b2; **g** — Bt–Amp andesite lithoclasts from volcanic conglomerate (PPL), ZM-1/c18, 1346–1351 m/b1; **h** — Cum-bearing andesite clast from sandy conglomerate (PPL), ZM-1/c12, 1046–1051 m/b1.

They contain white blasts (0.5–3 cm) made up of recrystallized Qz, Pl, minor Kfs or by aggregates of these minerals. The space between the blasts is occupied by microcrystalline Qz, Chl and by dispersed opaque minerals. At the depth of 2355 m light grey phyllonitic to porphyroblastic rocks with pink-coloured carbonate veins occur (Fig. 8). Less deformed parts have a similar composition as the underlying rocks, but the degree of Fs sericitization increases and the intensively coloured Chl is absent. The pseudomatrix is formed by sericite. In the intensively deformed parts the ribbons are formed by recrystallized Qz, moreover laminas of idiomorphic Tur (Table 2, Fig. 6a) and opaque minerals are found. Both sampled levels display cataclastic crushing. From the accessory minerals Zrn, Rt and Py occur.

The base of the Neogene fill is composed of poorly sorted conglomerates and sandstones (2350–2140 m, Fig. 7). Normal gradation, erosional surfaces, lamination and ripple cross-lamination is observed (Fig. 8). The diameter of the clasts does not exceed 10 cm. In the conglomerates grey micritic carbonates occur, which yield rare foraminifera and calcite veins. Other present carbonates yield pelmicrosparite, sparite to recrystallized textures. Carbonate breccia and carbonate siltstone clasts occur. It is important to note, that carbonate clasts are less rounded, than the siliciclastic lithoclasts. They are composed of granitoid to metagranitoid and sandstones. The large granitoid fragments are heavily shattered, and the fissures are filled with calcite (Calc). Sandstones and meta-sandstones are ranked to quartz arenite, arkose to meta-greywacke with sericitic pseudomatrix. Clasts corresponding to Bt schist are also found. Quartz phyllite, shale, chert and melaphyre are less abundant. Melaphyre clasts with intersertal and rarely diorite texture include Pl phenocryst in dark groundmass. Amygdales and pseudomorphs are filled by Qz and microcrystalline Qz (Fig. 6). Additionally, a fragment of Permian felsite with magmatically corroded Qz and a fragment of pseudotachylite is found. Mineral grains are mainly composed of polycrystalline Qz, Or, Pl and Tur. Carbonate cement is present in all samples. The overlying part from the depth of 2140–1930 m is dominated by mudstones and sandstones. The mudstones are commonly bioturbated and contain rare leaf (*Zelkova* sp.) and fish fossils (Pleuronectiformes; Zahradníková et al. 2013). In the sandstones two types of structures occur: the first is characterized by gradation and the second by horizontal and ripple-cross lamination (Fig. 8). Pillow structures and synsedimentary folds are abundant in both sandstone types. The grain composition is enriched by shales to phyllites and large leaves of Chl, Ms and Bt. In the binding material Glt and foraminifers occur. From volcanites, only one clast is observed, but the size of the clast does not allow its assignment to Paleozoic or Neogene volcanics. The carbonate cement is poikilitic in some samples, while clay intraclasts are common. In the depth of 1930–1650 m para-conglomerates (gravel: 14–25 %, sand: 49–56 %, lutite: 25–30 %) are present (Figs. 7, 8). Well rounded clasts are max. 3–5 cm in diameter and are accompanied by armoured mud intraclasts and synsedimentary fold structures. The debris composition is dominated by granitoids, additionally a small amount of white Neogene volcanic clasts are present. They are composed of Pl phenocryst in altered glassy groundmass. The remaining intervals were poorly sampled, or were not sampled at all. Nonetheless the SP and RT log trends can provide some data on the lithology, which is confirmed by the core 5 which drilled massive mudstones (Fig. 8).

Heavy minerals were analysed from five samples (depth 2240, 2160, 1960, 1760 and 1705 m). Their mineral composition is similar. Among transparent heavy minerals Grt (16–53 %) dominate, while Tur, St, Ap, Rt, Zrn are less abundant (< 8 %). Both dravite and schorl Tur are observed. Ilm creates 6–42 % and oxidized framboidal pyrites with minerals of limonite group create 5–26 %. Glt is present mainly in the depth of 2240–1960 m (5 to 6 %) and decreases in the depth of 1760–1705 m to < 1 %. In the first interval one magnesiochromite spinel ($Mg_{0.52}Fe^{2+}_{0.46}Mn_{0.01}Cr_{1.18}Al_{0.77}Fe^{3+}_{0.04}O_4$) is detected. On the other hand, Ep appeared in the second interval.

VR-1 well

Basement rocks drilled in the VR-1 well are composed of metamorphosed pink quartzites together with lila-brown shales and overlying dolomite with layers of black graphitic shale (Gaža 1968; Biela 1978a). From these rock types only the brecciated microcrystalline dolomite (Figs. 9, 10) is preserved.

Conglomerates from the base of the Neogene fill were not present in the archive (2460–2300 m). Only original petrografic analyses describing poorly rounded, variegated clasts (max. 3 cm in diameter) of siltstones, claystones, shales, sandstones and rare, limonitized diabase grains with ophitic texture were reported by Gaža (1968).

The overlying interval is marked by abundant epiclastic volcanic material (2300–1860 m). The sequence starts with normally graded conglomerates and sandstones with rounded clasts (Fig. 10). They pass into poorly sorted, coarse-grained sandstones with armoured mud intraclasts. The lower white and green coloured part (up to 2055 m) consists of rhyolitic vitroclasts, spherulites, spherulitized vitroclast, pumice, Kfs, Pl ($An_{23–29}$; Fig. 11, Table 3), Qz phenocrysts (observed magmatic corrosion) and rare heavily altered Bt (Fig. 6). This part also contains greenish crystalloclastic fine-grained tuff clasts, which rarely include vitroclasts and volcanic lithoclasts. These tuff fragments showed signs of deformation and bending around clastic grains. Non-volcanic lithoclasts are fairly rare. They are composed of granitoid, metaarkose, quartz arenite, phyllite/shale, Qz-mica schist, polycrystalline Qz and Zrn. At the depth of 2055 m, the composition of the volcanic material changes. Intermediate volcanic lithoclasts with porphyritic, intersertal and pilotaxitic texture dominate and lithoclasts with perlite texture are very rare. They are composed of Pl phenocrysts ($An_{40–63}$; Fig. 11, Table 3) and pseudomorphs after mafic minerals (Px?)±Bt (Fig. 6). From phenocrysts Qz, Bt, zonal and sieved Pl and pseudomorphs after mafic minerals

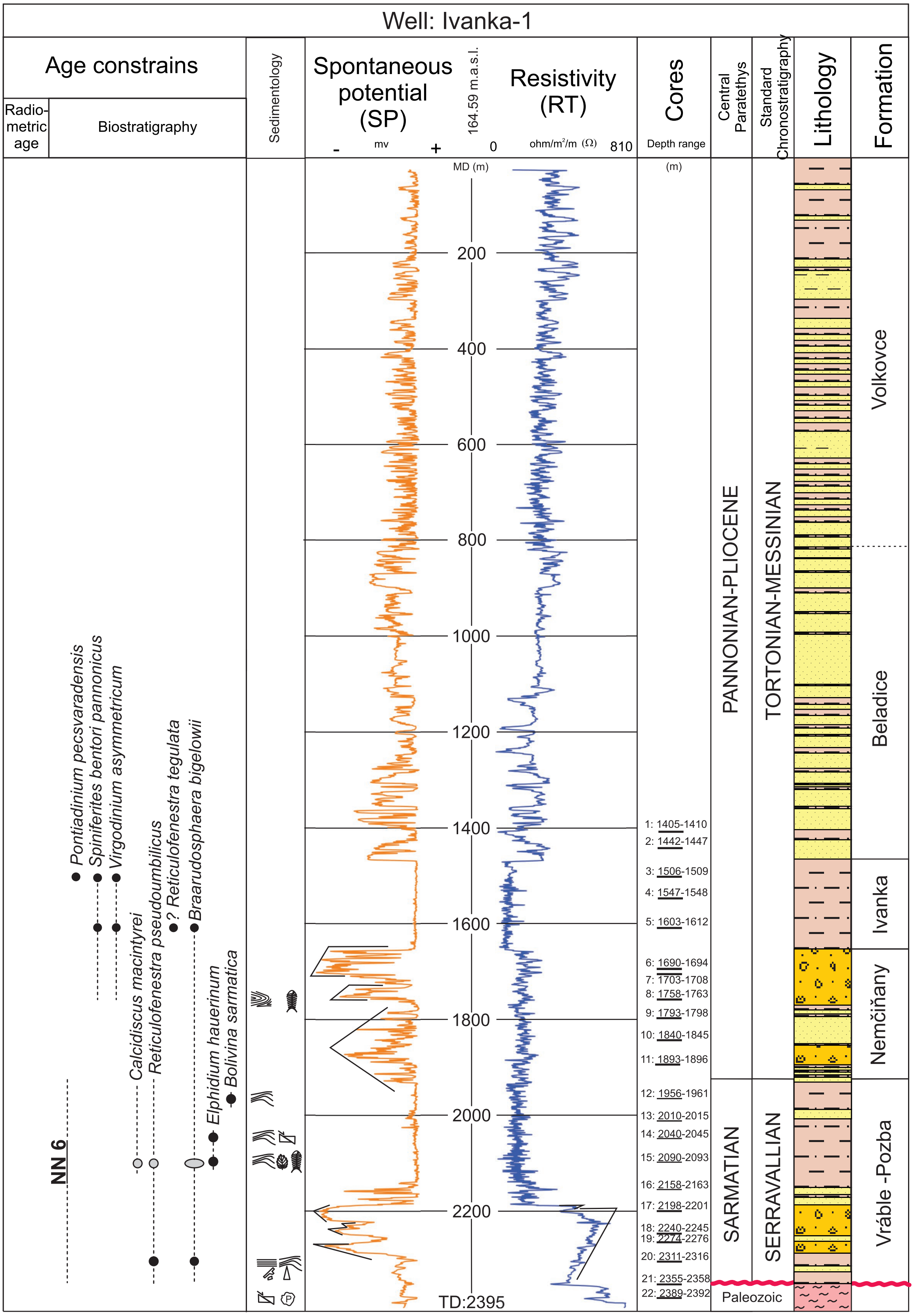

Fig. 7. IV-1 well table; for explanations see Fig. 4.

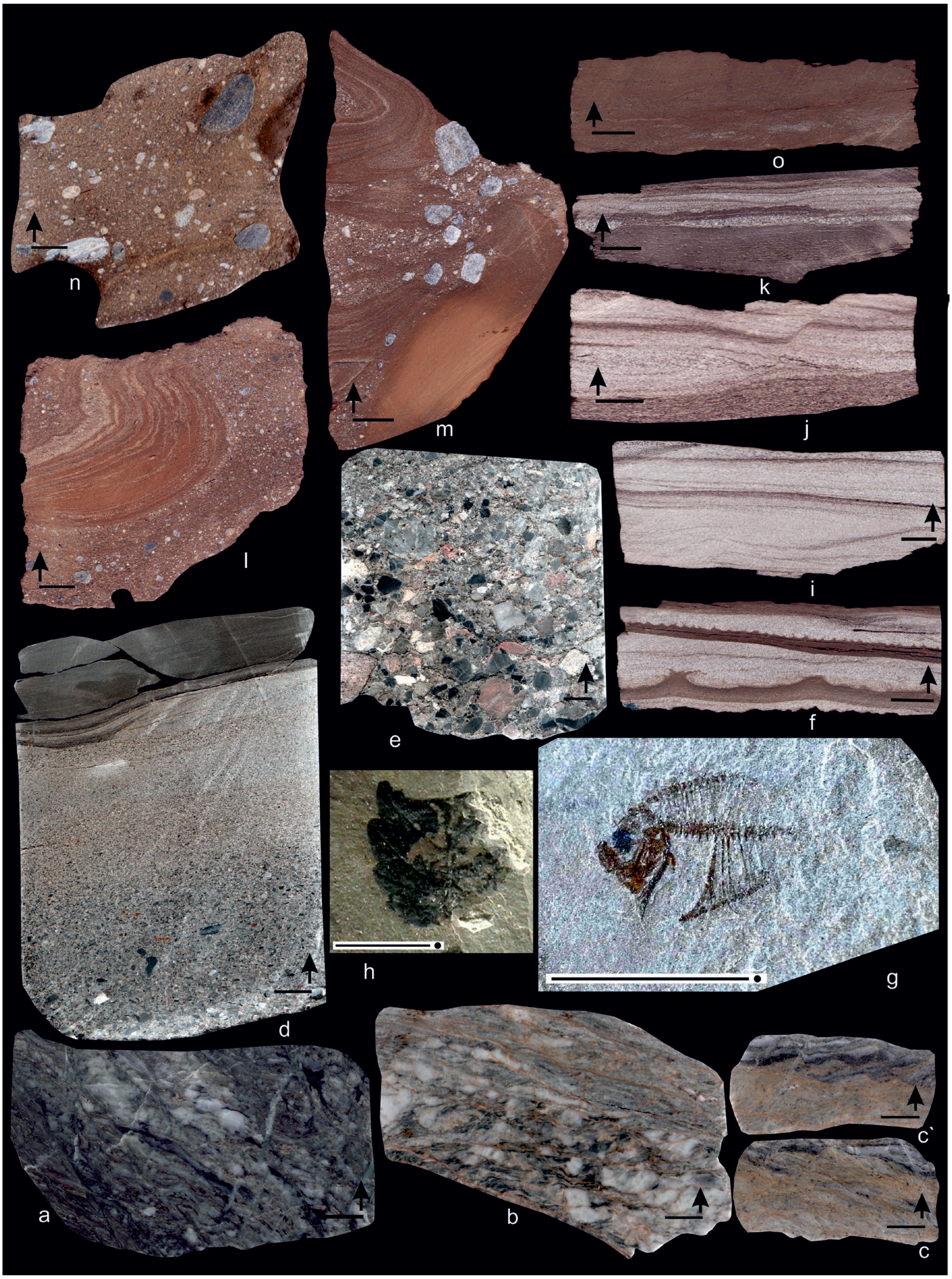

Fig. 8. IV-1 well core samples (for symbol explanations see Fig. 5): **a** — mylonite; IV-1/c22, 2389–2392 m/b1; **b, c** — mylonite; IV-1/c21, 2355–2358 m/b3; **d** — transition from graded conglomerate (up to 6 mm) through laminated sandstone to wavy ripples and laminated mudstone (gravity flow) IV-1/c20, 2311–2316 m/b3; **e** — graded conglomerate (up to 2 cm), IV-1/c20, 2311–2316 m/b3; **f** — heterolithic sediment including ripples with pillow structures and abundant carbonized plant fragments, IV/c16, 2158–2163 m/b2; **g** — fine-grained sandstone with Pleuronectiformes fish fossils (Zahradníková et al. 2013) IV-1/c15, 2090–2093 m/b3; **h** — mudstone with preserved *Zelkova* sp. carbonized leaves, IV-1/c15, 2090–2093 m/b1; **i** — flaser bedding with ripples draped by carbonized plant fragments. IV1/c15, 2090–2093 m/b3; **j** — wavy bedding with carbonized plant fragments and synsedimentary faults, IV-1/c14, 2040–2045 m/b1; **k** — heterolithic sediment with lenticular bedding; IV-1/c12, 1956–1961 m/b3; **l, m** — reddish para-conglomerate (up to 0.5 cm) with synsedimentary folds, IV-1/c8, 1758–1763 m/b5; **n** — reddish para-conglomerate (up to 1.5 cm clasts), IV-1/c7, 1703–1708 m/b2; **o** — massive mudstone, IV1/c7, 1703–1708 m/b2.

Table 2: Selected analyses of tourmaline (*calculated to stoichiometry) and allanite.

Well	Neogene fill							Mylonite basement			
	ZM-1		VR-1	MOJ-1			IV-1	IV-1/21			
	core	rim		core	rimI	rimII		core	rim	core	rim
Min.	Srl	Drv	Drv	Srl	Drv	Drv	Srl	Drv	Drv	Drv	Drv
SiO_2	36.63	36.70	36.82	36.19	36.64	37.98	34.54	36.60	37.65	37.88	37.13
TiO_2	0.53	0.66	0.44	1.77	0.87	0.05	0.29	0.16	0.22	0.14	0.15
Al_2O_3	29.28	32.73	34.98	28.69	32.33	32.05	33.25	32.24	31.91	32.72	32.41
Cr_2O_3	0.02	0.02	0.03	0.03	0.07	0.00	0.00	0.00	0.04	0.00	0.00
FeO	9.58	6.94	5.83	11.84	7.81	5.77	15.11	3.09	4.01	2.61	3.68
MgO	5.94	5.95	5.68	5.27	5.96	7.98	0.69	10.28	9.66	10.06	9.57
CaO	0.30	0.57	0.54	0.31	0.65	0.05	0.09	0.12	0.26	0.16	0.14
MnO	0.00	0.02	0.06	0.01	0.00	0.00	0.10	0.02	0.01	0.00	0.06
Na_2O	2.57	1.78	1.71	2.59	1.93	2.20	1.88	2.58	2.48	2.49	2.46
K_2O	0.02	0.01	0.04	0.03	0.01	0.00	0.06	0.02	0.02	0.03	0.06
F	0.00	0.00	0.00	0.00	0.00	0.00	0.27	0.00	0.00	0.00	0.00
Cl	0.01	0.00	0.01	0.01	0.00	0.00	0.01	0.00	0.00	0.01	0.00
H_2O*	3.59	3.67	3.74	3.59	3.68	3.73	3.40	3.70	3.74	3.77	3.72
B_2O_3*	10.40	10.64	10.83	10.42	10.67	10.80	10.24	10.71	10.84	10.92	10.77
Li_2O*	0.51	0.34	0.42	0.26	0.31	0.35	0.17	0.00	0.14	0.18	0.03
Total	*99.37*	*100.04*	*101.13*	*101.02*	*100.95*	*100.97*	*100.10*	*99.51*	*100.98*	*100.94*	*100.17*
O=F	0.00	0.00	0.00	0.00	0.00	0.00	0.11	0.00	0.00	0.00	0.00
Si	6.123	5.995	5.909	6.033	5.967	6.109	5.863	5.939	6.035	6.028	5.993
^{T}Al	0.000	0.005	0.091	0.000	0.033	0.000	0.137	0.061	0.000	0.000	0.007
B	3.000	3.000	3.000	3.000	3.000	3.000	3.000	3.000	3.000	3.000	3.000
^{Z}Al	5.769	6.000	6.000	5.638	6.000	6.000	6.000	6.000	6.000	6.000	6.000
Mg	0.231	0.000	0.000	0.362	0.000	0.000	0.000	0.000	0.000	0.000	0.000
Cr	0.000	0.000	0.000	0.000	0.000	0.000	0.000	0.000	0.000	0.000	0.000
Fe^{3+}	0.000	0.000	0.000	0.000	0.000	0.000	0.000	0.000	0.000	0.000	0.000
Al	0.000	0.295	0.524	0.000	0.172	0.075	0.515	0.103	0.030	0.138	0.158
Ti	0.067	0.081	0.054	0.222	0.107	0.007	0.036	0.020	0.026	0.016	0.018
V	0.000	0.000	0.000	0.000	0.000	0.000	0.000	0.000	0.000	0.000	0.000
Cr	0.002	0.002	0.004	0.004	0.009	0.000	0.000	0.000	0.006	0.000	0.000
Fe^{3+}	0.000	0.000	0.000	0.000	0.000	0.000	0.000	0.000	0.000	0.000	0.000
Mg	1.249	1.449	1.359	0.948	1.448	1.914	0.174	2.487	2.308	2.386	2.301
Mn	0.000	0.002	0.008	0.002	0.000	0.001	0.015	0.002	0.001	0.000	0.008
Fe^{2+}	1.340	0.948	0.782	1.651	1.064	0.776	2.145	0.419	0.538	0.347	0.497
Zn	0.000	0.000	0.000	0.000	0.000	0.000	0.000	0.000	0.000	0.000	0.000
Li*	0.342	0.222	0.269	0.174	0.200	0.228	0.114	0.000	0.092	0.113	0.017
Ca	0.053	0.099	0.092	0.056	0.113	0.009	0.017	0.020	0.045	0.027	0.024
Na	0.832	0.565	0.532	0.837	0.610	0.686	0.619	0.811	0.771	0.768	0.771
K	0.004	0.003	0.009	0.007	0.001	0.001	0.012	0.005	0.003	0.006	0.011
r	0.110	0.333	0.366	0.101	0.275	0.304	0.352	0.164	0.181	0.198	0.194
OH	3.998	4.000	3.999	3.998	4.000	4.000	3.853	4.000	3.999	3.998	4.000
F	0.000	0.000	0.000	0.000	0.000	0.000	0.144	0.000	0.000	0.000	0.000
Cl	0.002	0.000	0.001	0.002	0.000	0.000	0.003	0.000	0.001	0.002	0.000

Well	Neogene fill	
	VR-1	
	Aln	Aln
SiO_2	31.32	30.89
TiO_2	0.77	1.41
Al_2O_3	14.40	13.85
FeO	15.56	15.63
MgO	0.66	0.64
MnO	0.76	0.36
SrO	0.05	0.06
CaO	10.31	9.94
Na_2O	0.01	0.03
Y_2O_3	0.12	0.13
ThO_2	1.83	0.61
UO_2	0.04	0.01
La_2O_3	6.78	6.63
Ce_2O_3	11.43	12.30
Pr_2O_3	1.08	1.27
Nd_2O_3	2.89	3.77
Sm_2O_3	0.28	0.36
Eu_2O_3	0.40	0.37
Gd_2O_3	0.17	0.32
Tb_2O_3	0.05	0.04
Dy_2O_3	0.00	0.12
Er_2O_3	0.13	0.19
Tm_2O_3	0.03	0.06
Yb_2O_3	0.04	0.09
Lu_2O_3	0.19	0.24
Total	*99.31*	*99.32*
Si	2.996	2.981
^{T}Al	0.004	0.019
Al	1.619	1.556
Ti	0.056	0.102
Mg	0.095	0.091
Fe	1.245	1.262
Mn	0.062	0.030
Ca	1.056	1.027
Sr	0.003	0.003
Th	0.040	0.013
U	0.001	0.000
Ce	0.400	0.435
La	0.239	0.236
REE	0.183	0.238

filled by Chl are present. Chloritized tuffaceous matrix is responsible for the green-grey sediment colour and its share decreases upward. However, rhyolitic lithoclasts are still present. At the depths of 2055 m and 1904 m carbonatized tuffite layers are cut by multiple veins (Fig. 10).

The overlying heterolithic interval (1860–1310 m) is dominated by sandstones with occasional coal seams and abundant carbonized plant fragments. Within sedimentary structures lamination, ripple-cross lamination, small scale cross-beds, bioturbation, normal gradation, mud intraclasts and convolute bedding are observed, (Fig. 10). The amount of volcanic lithoclasts decreases, whereas content of stable minerals (Qz, Zrn, Tur, Rt, Grt) and non-volcanic rock fragment increases. The amount of the carbonate cement, sorting and roundness of grains increases as well. The composition of non-volcanic lithoclasts is enriched by micritic carbonates, cherts and fossil remnants. In the depth up to 1550 m Glt is documented.

In the depth of 1310–1250 m, a change in the lithological appearance is observed. This interval is composed of para-conglomerate to poorly sorted, coarse-grained sandstone with approximately 7 % gravel (max. 1 cm in diameter), which includes abundant cardiids (Fig. 10). The volume of the sandy and lutite fraction is the same (50 %). Sandy and gravelly layers are rarely supplemented by muddy intercalations. Clast composition remains the same.

The upper parts (1250–395 m) are characterized by alterations of mudstones and minor sandstones. The matrix is predominantly red in colour. Lamination, bioturbation, synsedimentary folds, carbonized plant fragments, leaves (*Ulmus pyramidalis*) and dreisenids are present (Fig. 10). The fine-grained sands consist of Qz, Fs, Ms, Chl and rarely observed carbonate crystals.

Heavy minerals were analysed from four sandy samples (depth 1450, 1305, 1250 and 950 m) and one lutite sample (depth 500 m). Mineral composition is nearly identical in all samples, but representation of individual minerals at the 500 m depth is significantly affected by overall grain-size of the sample. Grt (7–44 %) and Ilm (18–43 %) dominated in the sandy samples; in the lutite sample Grt create 3 %. Ap, St, Tur (dravite), $La_{0.21\text{-}0.24}Ce_{0.40\text{-}0.43}$ allanite (Table 2), Zrn and Rt did not

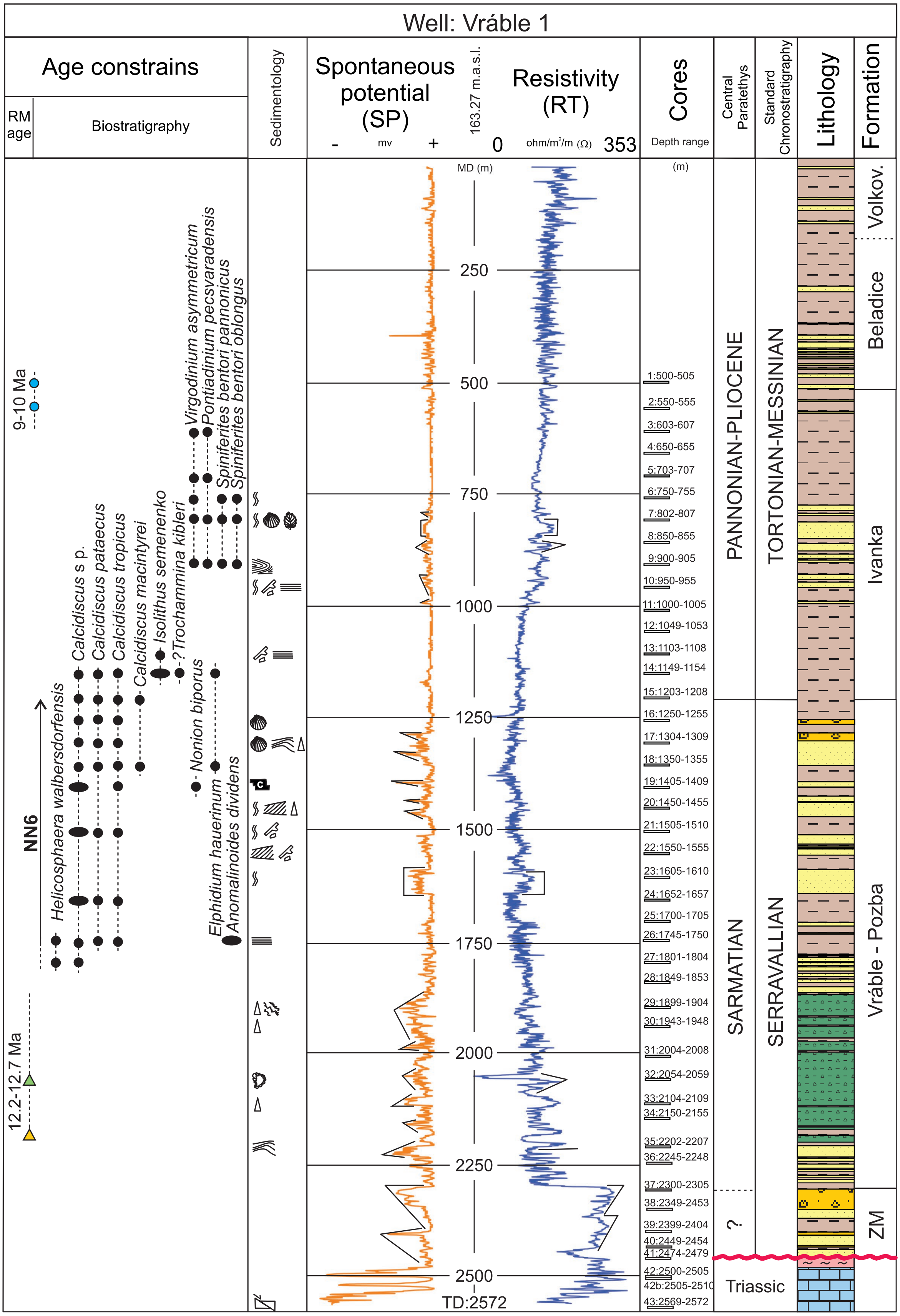

Fig. 9. VR-1 well table; for explanations see Fig. 4.

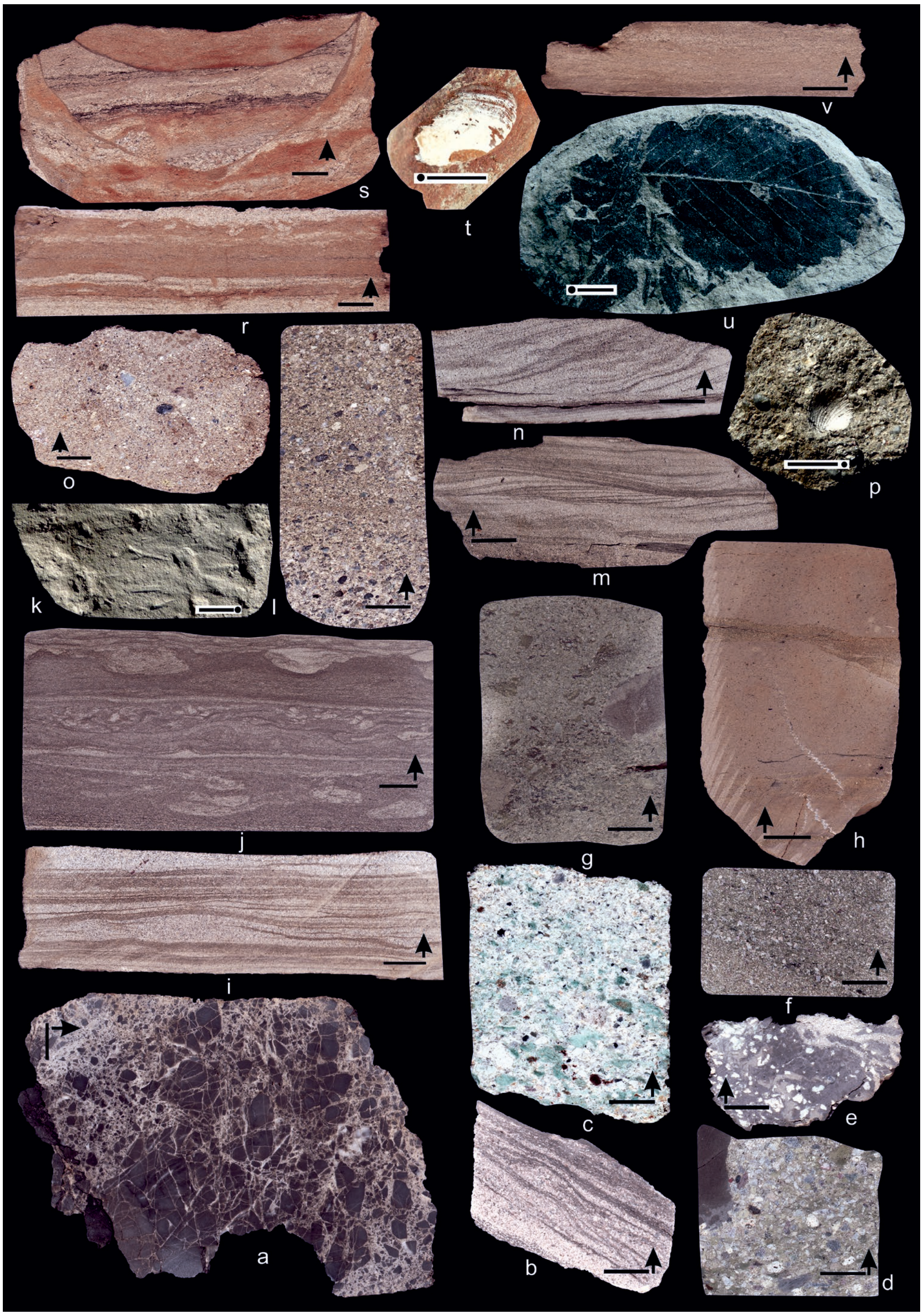

Fig. 10. VR-1 well core samples (for symbol explanations see Fig. 5): **a** — tectonized carbonate breccia, VR-1/c43, 2569–2572 m/b5; **b** — wavy beddings with carbonized plant fragments, VR-1/c35, 2202–2207 m/b3; **c** — green to white, normally graded volcanic conglomerate. Clasts reached up to 6 mm in diameter; VR-1/c33, 2104–2109 m/b3; **d** — greenish volcanic conglomerate with armoured mudstone intraclasts, VR-1/c32, 2054–2059 m/b2; **e** — carbonized tuffite, VR-1/c32, 2054–2059 m/b2; **f** — greenish, coarse-grained volcanic sandstone; VR-1/c30, 1943–1948 m/b2; **g** — greenish para-conlomerate with mudstone intraclasts; VR-1/c29, 1899–1904 m/b2; **h** — tuffite cut by calcite veins; VR-1/c29, 1899–1904 m/b2; **i** — heterolithic sediment with wavy to lenticular bedding; VR-1/c26, 1745–1750 m/b2; **j** — heterolithic sediments with convolute bedding and pillow structure; VR-1/c23, 1605–1610 m/b1; **k** — fine-grained sandstone with trace fossil on the bedding planes, VR-1/c21, 1505–1510 m/b2; **l** — fine-grained conglomerate (up to 3 mm) to coarse-grained sandstone, VR-1/c20, 1450–1455 m/b3; **m** — heterolithic sediment with flaser bedding and abundant carbonized plant fragments, VR-1/c20, 1450–1455 m/b2; **n** — heterolithic sediment with flaser bedding and abundant carbonized plant fragments; VR-1/c20, 1450–1455 m/b5; **o** — para-conglomerate (up to 5 mm),VR-1/c17, 1304–1309 m; **p** — conglomerate (up to 3 mm) with fragments of *Cardiidae* bivalves, VR-1/c16, 1250–1255 m/b3; **r** — reddish, bioturbated, heterolithic sediment with carbonized plant fragments. VR-1/c10, 950–955 m/b1; **s** — reddish, heterolithic sediment with synsedimentary folds and carbonized plant fragments. VR-1/c9, 900–905 m/b1; **t** — reddish mudstone with *Dreissenid* bivalves. VR-1/c7, 802–807 m/b3; **u** — fine-grained sandstone with preserved carbonized *Ulmus pyramidalis* leaves, VR-1/c7, 802–807/b4; **v** — reddish mudstone, VR-1/c1, 500–505 m/b2.

exceed 3 %. The amount of framboidal pyrite and limonite minerals increases upward from 4 % (in the depth 1450 m) to 55 % (in the depth 1250 m). Samples from the depth of 950 and 500 m no longer contain pyrite, but the sample from the depth of 950 m is leucoxenized and the content of limonite minerals is 62 %. In contrast, the lutite sample from the depth of 500 m has only 7 % of limonite minerals. Associations of the sandy samples are completed by monazite and rock fragments formed by $Na_{0.40}Ca_{0.54}$-rich mica with inclusions of chloritoid and staurolite (Fig. 12).

ZM-1 well

The basement rocks in the ZM-1 well were not present in the repository. However, in the original report (Gaža 1970) grey metamorphosed arkose with carbonate veins (depth below 1956 m) is assigned without a doubt to the Paleozoic basement (Fig. 13). The lower limit of the Neogene fill in the ZM-1 well is questionable due to the lack of the disputed well cores (Fig. 13). From this interval, only a core from the depth of 1711–1708 m is preserved, which has similar character as sedimentary rocks from the depth of 1558–1448 m. These sediments are represented by fine-grained conglomerates, sandstones and mudstones. In the grey mudstones, synsedimentary folding, abundant carbonized plant fragments and red mottles are observed (Fig. 14). The mudstones are often cut by scours and filled with fine-grained conglomerates. The conglomerate and light coloured sandstones are normally graded. Clasts are poorly rounded and locally poorly imbricated. In their composition the Qz, Qz-sericitic and carbonate shale lithoclasts strongly dominate. Altered granitoids to meta-granitoids, meta-greywacke, meta-arkose, chert/felsite, quartz arenite, arkose, lithic sandstone and micritic to recrystallized carbonates are also included. In the upper part (above 1495 m) altered volcanic lithoclasts appear and their volume

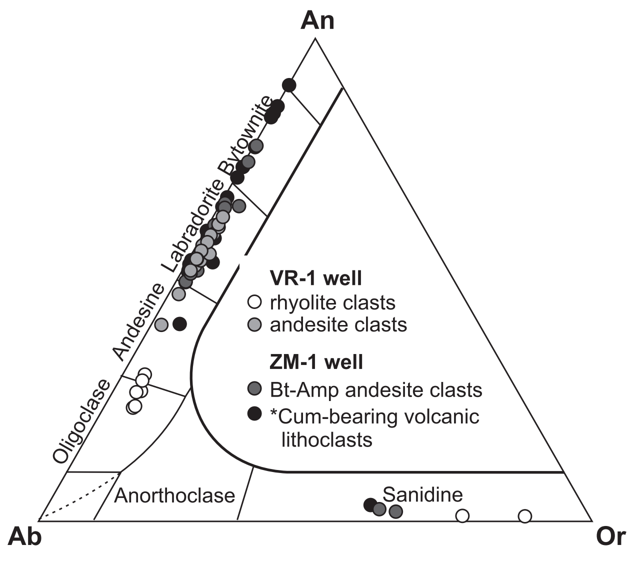

Fig. 11. Composition of feldspars in volcanic lithoclasts from ZM-1 and VR-1 well. * data taken from Šarinová & Rybár (2018).

increases upward. From mineral grains altered Fsp, Bt, Zrn and opaque minerals occur. Some granitoid grains are carbonatized.

A significant change in the modal composition is observed at a depth of 1410–1007 m. At the base of the interval (depth 1405–1410 m) weakly consolidated, greenish, massive volcanic sandstones with tuffaceous matrix are present (gravel 1–4 %, sandy fraction 44–55 %, lutite fraction 44–53 %). Volcanic origin is represented by altered volcanic lithoclasts, vitroclasts and Pl. Mafic minerals except altered Bt are not preserved. Inside these sandstones, well sorted polymict conglomerates with normal to inverse gradation and well rounded pebbles (1–2 cm diameter) are present (Fig. 14). They contain poikilitic calcite cement. Abundant volcanic lithoclasts yield intersertal and porphyritic texture with Pl phenocrysts and pseudomorphs after mafic minerals (Px±Amp) often filled by calcite in microlithic glass. Nonvolcanic lithoclasts in both types are composed of quartz arenite, arkose, meta-arkose, greywacke with strong ore pigment, lithic sandstone, siltstone and altered granitoids. These volcanic sandstones pass into grey mudstones. In the mudstone, intercalation of coarse-grained volcanic conglomerate (depth 1351–1346 m) and bentonite (1310–1305 m) appears (Fig. 14). Volcanic conglomerate with subrounded to poorly rounded pebbles cannot be clearly classified because of the ratio between core diameter (10 cm) and the clast diameter (up to 6 cm). The conglomerate is unsorted and is formed entirely by volcanic lithoclasts of andesite to dacite with porphyritic texture. The composition of the lithoclasts and matrix is approximately the same. Pronounced rusty colour of the matrix is a result of a stronger alteration. Lithoclasts with microcrystalline groundmass are light pink to grey and yield large phenocryst (about 0.5 cm) of reddish-brown, idiomorphic Bt, and Pl ($An_{74\text{-}65}$ in the core to An_{51} in the rim; Fig.11, Table 3). Opacitic Amp phenocrysts are dominantly of magnesio-hastingsite composition, less frequently of magnesio-ferri-hornblende composition (Šarinová & Rybár 2018). They are often replaced by secondary minerals. Rare magmatically corroded Qz, Kfs and augite are also present (Fig. 6). The white bentonite layers contain glass shards, Qz, Pl and Bt in smectite matrix. Above the bentonite, mudstones dominate and include rare, graded sandstone layers. Coarse-grained sandstones with poikilitic carbonate cement (1255 m) contain well-rounded cloudy volcanic epiclasts, shale, granitoid, carbonates, quartz arenite, arkose, Qz, sericitized Or, Pl, Bt and Tur. At the depth of ~1100 m fine-grained deposition is terminated by the second layer of coarse-grained volcanic conglomerate (the clasts reach up to ~10 cm; Fig. 14). Their composition corresponds to the composition of volcanic conglomerate from the depth of 1350 m, but one green clast of an andesitic tuff is also found. The volcanic conglomerate passes into poorly sorted, chaotic, rusty coloured, sandy volcanic paraconglomerate and coarse-grained sandstone (gravel: 4–11 %, sand: 39–60 %, lutite: 28–57 %). These chaotic conglomerates are composed of rounded andesite clasts, heavily altered volcanic lithoclasts and elongated mud intraclasts (Fig. 14). Heavy synsedimentary deformation and poorly preserved ripples are also documented. The diameter of lithoclasts decreases upward from 5 to 2 cm. Well rounded, lithified clasts of older volcanic rocks are similar to those in the underlying volcanic lithoclasts. Strongly altered, friable clasts with the rusty-brown, hyaline to pilotaxitic volcanic groundmass contain phenocryst of Bt, Pl, Amp, Px and

Table 3: Selected analyses of feldspar from volcanic lithoclasts (Phen.–phenocrysts, matrix–crystals from groudmass).

well	VR-1 rhyolite clasts				VR-1 andesite clasts							ZM-1 Bt-Amp andesite/dacite clasts								
depth	2104 - 2109 m				1450 - 1250 m							1346 - 1351 m				1099 - 1104 m				
type	Kfs Phen.	Kfs Phen.	Pl Phen.	Pl Phen.	Pl Phen.	Pl Phen.	Pl matrix	Pl Phen.	Pl matrix	Pl Phen.	Pl Phen.	Pl Phen.	Pl Phen.	Pl Phen.	Pl matrix	Pl Phen.	Pl Phen.	Kfs Phen.	Pl matrix	Kfs matrix
SiO_2	64.74	64.62	61.49	62.42	54.94	55.32	53.40	53.55	54.07	53.77	55.04	51.77	55.69	49.04	55.77	52.50	48.32	65.08	54.18	65.24
Al_2O_3	18.55	18.20	23.78	23.12	27.37	27.41	27.48	28.90	28.16	28.22	28.10	30.26	27.97	32.54	28.43	29.78	32.30	20.29	28.66	20.79
SrO			0.13	0.11	0.05	0.03	0.08	0.06	0.07	0.05	0.12	0.09	0.11	0.11	0.09	0.10	0.08		0.07	
FeO	0.05	0.08	0.12	0.11	0.91	0.57	1.04	0.39	0.81	0.79	0.22	0.44	0.18	0.28	0.41	0.34	0.48	0.27	0.51	0.24
MgO	0.00	0.03	0.04	0.03	0.02	0.02	0.06	0.00	0.02	0.04	0.00	0.03	0.00	0.00	0.02	0.04	0.04	0.00	0.03	0.02
BaO	0.39	0.25																0.89		0.47
CaO	0.13	0.15	5.55	4.79	11.17	10.80	11.62	12.11	11.89	12.02	11.17	13.68	10.59	15.90	11.11	12.90	16.09	0.29	11.15	0.46
Na_2O	2.58	1.29	7.76	8.02	5.01	5.10	4.77	4.32	4.61	4.38	5.02	3.61	5.67	2.93	5.38	4.38	2.47	3.78	4.95	4.15
K_2O	12.98	14.56	0.90	0.89	0.41	0.34	0.39	0.33	0.28	0.27	0.23	0.60	0.30	0.10	0.47	0.21	0.09	10.63	0.37	10.20
Total	*99.43*	*99.17*	*99.78*	*99.49*	*99.88*	*99.60*	*98.83*	*99.67*	*99.90*	*99.55*	*99.90*	*100.48*	*100.52*	*100.89*	*101.67*	*100.24*	*99.87*	*101.24*	*99.91*	*101.58*
Si	2.987	3.000	2.744	2.784	2.495	2.509	2.459	2.435	2.457	2.451	2.488	2.352	2.502	2.231	2.484	2.383	2.223	2.936	2.456	2.921
Al	1.008	0.996	1.251	1.215	1.465	1.465	1.492	1.549	1.508	1.516	1.497	1.621	1.481	1.745	1.492	1.593	1.751	1.078	1.531	1.097
Sr			0.003	0.003	0.001	0.001	0.002	0.002	0.002	0.001	0.003	0.002	0.003	0.003	0.002	0.003	0.002		0.002	
Fe	0.002	0.003	0.004	0.004	0.034	0.022	0.040	0.015	0.031	0.030	0.008	0.017	0.007	0.011	0.015	0.013	0.018	0.010	0.020	0.009
Mg	0.000	0.002	0.003	0.002	0.002	0.001	0.004	0.000	0.001	0.002	0.000	0.002	0.000	0.000	0.001	0.003	0.003	0.000	0.002	0.001
Ba	0.007	0.005																0.016		0.008
Ca	0.007	0.007	0.265	0.229	0.543	0.525	0.573	0.590	0.579	0.587	0.541	0.666	0.510	0.775	0.530	0.627	0.793	0.014	0.541	0.022
Na	0.231	0.116	0.671	0.693	0.441	0.449	0.426	0.381	0.406	0.387	0.440	0.318	0.494	0.258	0.465	0.385	0.220	0.330	0.435	0.360
K	0.764	0.862	0.051	0.051	0.023	0.020	0.023	0.019	0.016	0.016	0.014	0.035	0.017	0.006	0.026	0.012	0.006	0.612	0.021	0.582
cat. sum	5.006	4.991	4.992	4.981	5.005	4.992	5.019	4.991	5.000	4.992	4.991	5.014	5.014	5.028	5.016	5.019	5.015	4.996	5.007	5.002

probably orthopyroxene pseudomorphs filled by secondary minerals (Šarinová & Rybár 2018). The sandy matrix additionally includes Pl, Bt, Amp, Px, vitroclastic and crystalloclastic tuff clasts, arkose, granitoid, shale and polycrystalline Qz. The interval is closed by layered pale grey mudstone. Another significant change in the composition of sediments is observed in the depth of 1000–700 m. From the coarse clastic interval the core from the depth of 954–959 m was only available. Laminated sandstone with indistinct ripples, and abundant carbonized plant fragments, occurs together with poorly sorted conglomerate with synsedimentary folds and erosional contacts (Fig. 14). In this interval, altered volcanic lithoclasts are represented only by a small percentage. The dominating non-volcanic lithoclasts are composed of altered granitoid, mylonite, Qz to Qz–Ser shale, sandstone, Qz, Kfs, Pl and chloritized Bt. The drilling report (Gaža 1970) of several consecutive cores describes 3 to 10 cm long clasts composed of shale/phylite, quartz arenite, granitoid, greywacke and volcanite. A fine-grained interval follows in the depth of 700–340 m and is dominated by laminated mudstones with minor carbonized plant fragments. In the depth of 551–556 m a layer of poorly sorted, coarse-grained, sandstone to graded conglomerate is documented. Fine-grained conglomerate with crystalline carbonate cement showed a similar composition as the previous sample.

Heavy minerals were analysed from sandstones (1450 m) and volcanic sandstones to sandy conglomerates (1410 m, 1050 m and 1005 m). During the validation of mineral composition by microprobe, the polished section from the depth of 1450 and 1410 m contained only a small number of picked grains. From transparent minerals Ap 4–6 % dominated, Grt makes up 1–6 % and Tur 1–3 %. Zrn, Rt, Sp and Cpx (augite) are also present. One Tur with schorl core and dravite rim is part of a lithoclast consisting of Qz, Ms, Ab and Ap (Fig. 12). Sandstone from the depth of 1450 m consists of 71 % of limonite minerals, 12 % of pyrite (including framboidal) and 1 % of Ilm. On the other hand, volcanic sandstone from the depth of 1410 m is composed of 25 % of Ilm, 18 % of limonite and limonitized pyrite and idiomorphic Bt (37 %). Volcanic sandstones to conglomerates from the depth of 1050 m and 1005 m contain different amphibole rich associations (47–79 %). The associations are completed by Ilm together with Mag (16–45 %), Py (2–7 %), Ap (1–3 %), Px (1.6 %), Zrn, Tur, Rt, Ttn and Grt (less than 1 %). The composition of Amp (cummingtonite, magnesio-hornblende, magnesiohastingsite) and Px (augite) was published by Šarinová & Rybár (2018).

Garnet

Garnets were present in all samples, therefore they were selected for further study. The ZM-1 well is not statistically evaluated, since only one Grt was analysed. Grt are divided into seven groups based on different molecule composition (Fig. 15): a) $Alm_{24}Sps_{65}$ from MOJ-1 clearly corresponds to a granite source; b) $Prp_{11\text{-}21}Alm_{69\text{-}82}$ are abundant and contain inclusions of Chl, Rt and Zrn. They correspond to fields of

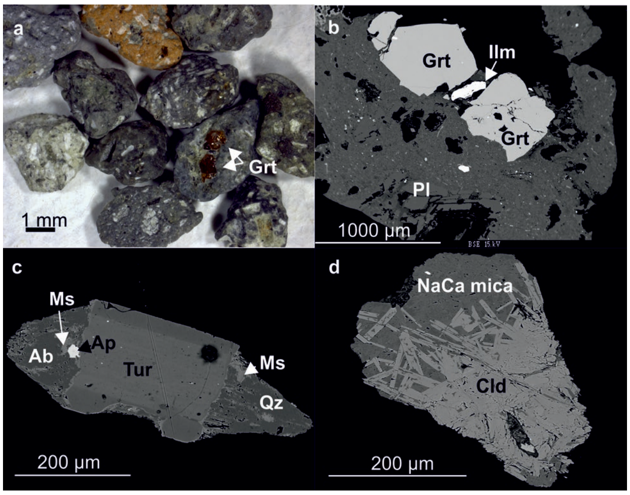

Fig. 12. a — andesite volcanic lithoclasts from the VR-1 well (1250–1309 m); **b** — detail of andesite clasts with Grt (BSE); **c** — metapelite clasts with zonal Tur (ZM-1, BSE); **d** — mica with Cld, VR-1/c20, 1450–1455 m.

granitoids and orthogneisses (Fig. 15); c) $Prp_{21\text{-}31}Alm_{63\text{-}68}$ indicate more Mg-rich provenance from gneiss (Suggate & Hall 2014; Fig. 15); d) $Prp_{7\text{-}18}Sps_{29\text{-}40}Alm_{41\text{-}43}$ (two Grt from MOJ-1) compositionality corresponds to Bt gneiss of the Tribeč Mts. (Ivanička et al. 1998); e) $Grs_{8\text{-}24}Alm_{52\text{-}83}$ composition is typical for low grade metapelite to amphibolite (Suggate & Hall 2014; Fig. 15). This group yields inclusions of Zrn, Al_2SiO_5, Ilm, Qz and Chl; f+g) $Grs_{9\text{-}24}Prp_{10\text{-}21}Alm_{59\text{-}69}$ with inclusion of Amp, Rt and Bt attributed to Neogene volcanic source or metabasites. This group yields Grt from the volcanic lithoclast of the VR-1 well (Fig. 12). A slightly different projection of the six Grt (f group) from the MOJ-1 and VR-1 wells (Fig. 15) is caused by low content of Sps molecule (< 2 %). Sps molecule in the g group varies from 2.2 to 10 %, with the highest peak in-between 4 to 6.5 %. Two Grt from the f group also contain $Prp_{21\text{-}31}$ (VR-1, MOJ-1), which can indicate an ultrabasic source (Suggate & Hall 2014).

Interpretation

Provenance

The wide spread late Badenian–Sarmatian sediments are limited by the Mojmírovce fault zone (e.g., Biela 1978a; Hók et al. 1999). The composition of non-volcanic sediments from the basal part of the Neogene fill is generally identical in all the analysed wells, but variation in the volume of individual lithotypes occurs. The tectonically disturbed granitoid clasts without Bt from the IV-1 well correspond to the leucocratic granite forming the basement of the MOJ-1 well. Leucocratic granites are typical for the top of granitoid plutons and their remnants are preserved in the Tribeč part of the Tribeč Mts. (Ivanička et al. 1998). According to the MOJ- 56, 57, 65 wells (Biela 1978a), the footwall of the Mojmírovce fault zone (Fig. 1) was built up by granitoids, which formed the source before the Pannonian (Tortonian). The higher content of granitoid clasts in the VR-1 well can be explained by erosion of the Tribeč Mts. or denudation of Cenozoic granitoids during the development of the Štiavnica stratovolcano (Konečný et al. 1998). Due to small areas of exhumation of Cenozoic granitoids, the source in these granitoids cannot be fully excluded, but it is unlikely. Provenance of the Bt gneisses observed in the IV-1 well and described in the IV-4 and 6 wells (Čermák 1976c, 1977a) can be derived from the Tribeč Mts. (Ivanička et al. 1998). Arkose, arkosic meta-greywacke, shale, melaphyre and rare paleorhyolite clasts indicated the presence of Paleozoic sediments in the source area. Arkosic metagreywacke can be derived from the Paleozoic cover unit of the Central Western Carpathians. Presence of non-metamorphosed arkose and melaphyre lithoclasts is typical for the Permian sequence of the Hronic units. These rocks outcrop in the Northern, Rázdiel part of the Tribeč Mts. (Vozárová & Vozár 1988). On the other hand, quartz arenite, greywacke, clay-sericitic shales and melaphyre layers were also described from the pre-Cenozoic basement of the Pohronský Inovec Mts. and vicinity (GK-5, 6, 12, 13, 14, PKŠ-1, VIK-1 wells; Biela 1978b; Fusán et al. 1987a,b). In this area, Paleozoic complexes are covered mainly by volcanics of the 4th stage of the Štiavnica Stratovolcano. This does not exclude provenance from this area, since the onset of the volcanic activity is associated with the end of deposition of non-volcanic sediments. From this point of view, the transport direction from the NE is obvious, especially in the ZM-1 well, where shale fragments dominate. In addition, the presence of the lithoclast with tourmaline (Fig. 12) in the heavy fraction of the ZM-1well (depth 1450 m) showed that the non-volcanic material comes from the first cycle of erosion. The abundant fragments of pink-coloured quartz arenite to subarkose can be attributed to the Lower Triassic of the Lúžna Fm., as well as to the Upper Triassic of the Carpathian Keuper Fm. (Ivanička et al. 1998). Both formations are present in the Tribeč Mts., but the pink-coloured subarkose to arkose and violet-coloured claystone (Gaža 1968) of the Carpathian Keuper Fm. (Biela 1978a) was also described from the top of the Pre-Cenozoic basement of the Vr-1 well. Their presence in the immediate basement suggests that they could form the margin of the depocentre. Therefore, the provenance of pink quartz arenite to subarkose can be found on the SW, as well as on the N rim of the depression. Micritic carbonates with small amounts of allochems are typical for the Triassic. At present such carbonates emerge to the surface in the Tribeč Mts. In addition, carbonate and shale alternations were described in MOJ-7, 8 and 29 wells which are located N and NW from the MOJ-1 and IV-1 wells (Biela 1978a; Fusán et al. 1987b; Fig. 1). The Mesozoic basement in these wells is covered only by Pannonian sediments, which means that carbonates formed the margin of the depression during the Sarmatian (late Serravallian) time. Towards the south, carbonate rocks were also found in the basement of the VR-1, POZ-1, 2, 4 and Podhájska-1 wells (Biela 1978a). In this case, carbonates are covered by sediments of late

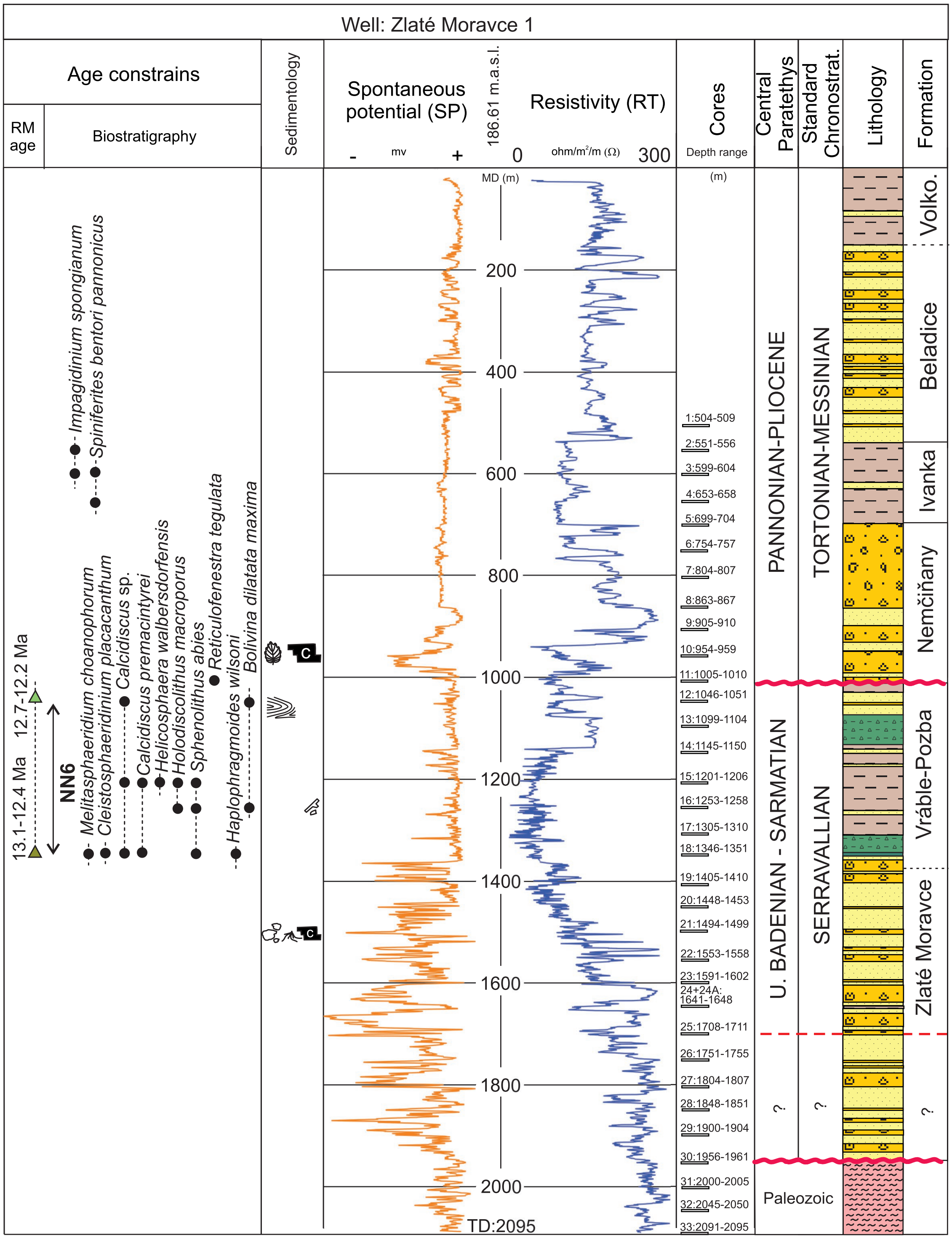

Fig. 13. ZM-1 well table; for explanations see Fig. 4.

Badenian–Sarmatian (Serravallian) age, but they could have been locally exposed. The interesting information is the higher angularity of carbonate clasts relative to siliciclastic lithoclasts in the IV-1 well. The same data are mentioned in the original drilling report of the IV-3, 5 and 6 wells (Čermák 1976a, b, c). The IV-6 well also contains intercalations of carbonate breccias (Čermák 1976c). The higher angularity of the carbonate debris points to a short transport distance in comparison to the silicate rock fragments. Proximity of the Mojmírovce fault system allows us to interpret clast angularity as a tectonically derived admixture. In general, we obtain an image of the dominant transport direction from E-NE, which was supplemented by material derived from the footwall of the Mojmírovce fault zone.

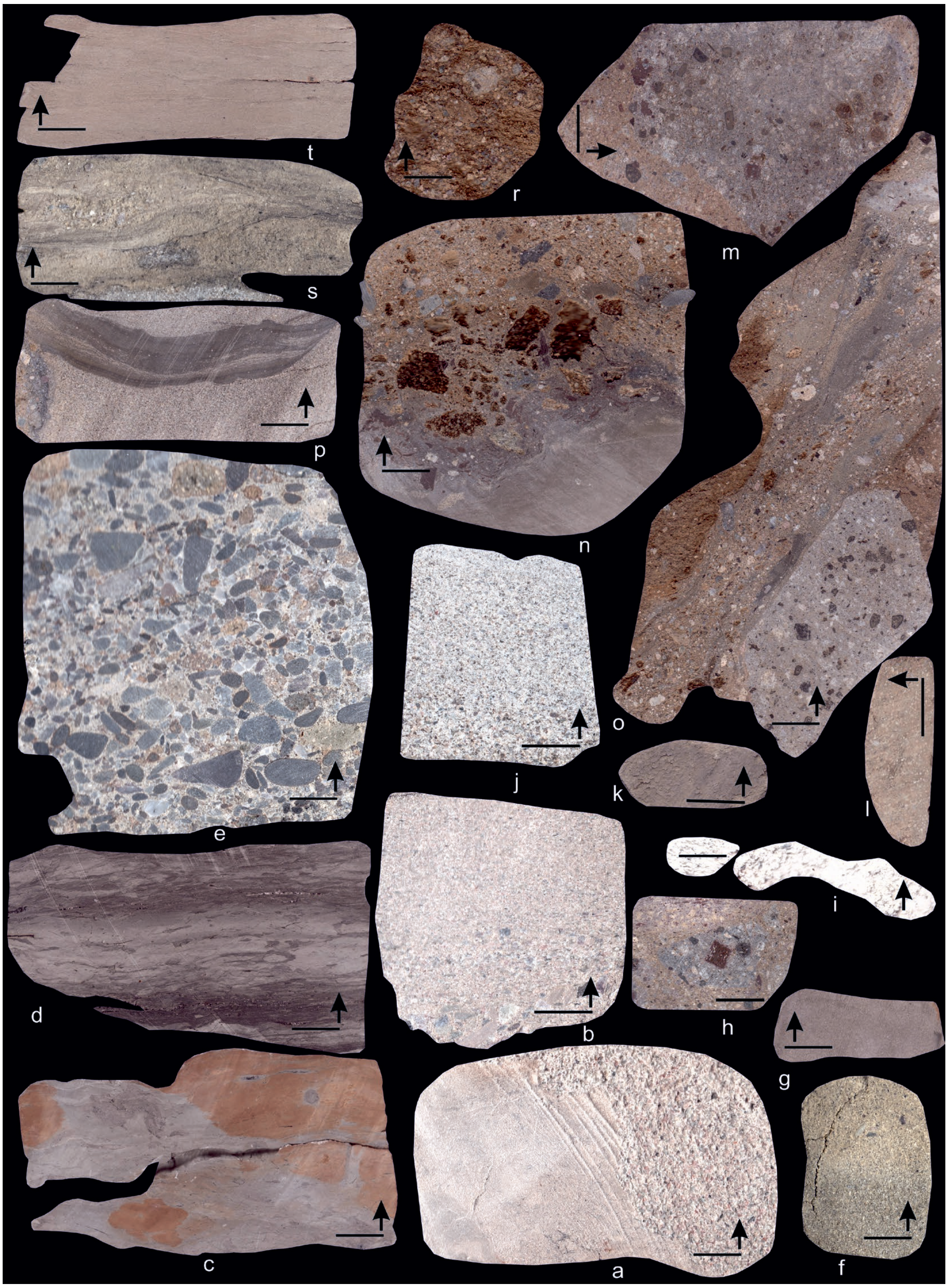

Fig. 14. ZM-1 well core samples (for symbol explanations see Fig. 5): **a** — massive mudstone cut by a scour filled by coarse-grained sandstone, ZM-1/c25, 1708–1711 m; **b** — normally graded conglomerate (up to 1 cm) to coarse-grained sandstone, ZM-1/c22, 1553–1558 m; **c** — mudstone with red mottles and carbonized plant fragments. ZM-1/c21, 1494–1499 m/b3; **d** — mudstone with abundant carbonized plant fragments, ZM-1/c21, 1494–1499 m/b2; **e** — normally graded conglomerate (up to 1.5 cm), ZM-1/c19, 1405–1410 m/b4; **f** — greenish, coarse-grained sandstone, ZM-1/c19, 1405–1410 m/b4; **g** — massive mudstone, ZM-1/c18, 1346–1351 m/b3; **h** — volcanic conglomerate, ZM-1/c18, 1346–1351 m/b1; **i** — bentonite, ZM-1/c17, 1305–1310 m/b4; **j** — normally graded, coarse to fine-grained sandstone with horizontal lamination at the top (gravity flow), ZM-1/c16, 1253–1258 m/b2; **k** — massive mudstone, ZM-1/c15, 1201–1206 m/b1; **l** — coarse-grained sandstone, ZM-1/c14, 1145–1150 m/b2; **m** — volcanic conglomerate, ZM-1/c13, 1099–1104 m/b4; **n** — contact of plastically deformed mudstone and conglomerate with strongly altered volcanic lithoclasts (up to 1.5 cm), ZM-1/c12, 1046–1051 m/b3; **o** — para-conglomerate with synsedimentary folds, ZM-1/c12, 1046–1051 m/b; **p** — medium grained sandstone with synsedimentary folds. ZM-1/c12, 1046–1051 m/b4; **r** — volcanic conglomerate, ZM-1/c11, 1005–1010 m/b3; **s** — greenish muddy sandstone with carbonized plant fragments and indistinct ripples, ZM-1/c10, 954–959 m/b5; **t** — massive mudstone, ZM-1/c2, 551–556 m/b3.

Different, finer grained development of basal sediments from the MOJ-1 well can be attributed to the position on a basement elevation of the Tribeč Mts. The high content of monocrystalline Qz and the very low amount of mica indicates that the granitoid source is similar to that of the underlying granite. The second major source is represented by carbonates. Both rock types can be linked to the Tribeč Mts., which confirms a local provenance.

In the MOJ-1 and IV-1 wells only a minor change of provenance was observed upwards. This is documented by large Bt, Bt-granitoid debris and by higher amounts of shale to phyllite clasts. The occurrence of granitoids with Bt indicates an increase in the influence of the Tribeč Mts. provenance. The shale debris generally means a relatively near source area, because of their rapid mechanical decay. They can still be derived from the basement, which was exhumed on the footwall of the Mojmírovce fault zone.

The admixture of volcanic material appears in sediments of late Badenian–Sarmatian (Serravalian) age, mainly in the eastern to central part of the depression (ZM-1 and VR-1 wells). In the ZM-1 well, a gradual transition from non-volcanic to volcanic epiclastic sediments manifested by an increase in volume of volcanic clasts was observed. Volcanic sandstones and andesite pebbles (1405–1410 m) indicate reworking of volcanites from the 1st stage of the Štiavnica Stratovolcano development. Based on mineral composition and felsic, microlithic groundmass the coarse-grained Bt–Amp±Px andesite to dacite conglomerate (1405 m, 1100 m) can be linked to the Studenec Fm. (3th volcanic stage; Šarinová & Rybár 2018). Today the Studenec Fm. outcrops on the surface between Nová Baňa town and Stará Huta village (Fig. 1; Konečný et al. 1998). Mudstone and sandstone intercalations from in-between volcanic conglomerates (1405–1100 m) indicate calming of volcanic activity and recycling of older deposits. Based on the fossil residues recycling of Oligocene, Cretaceous (Ozdínová 2012) and Badenian sediments is proved. The presence of strongly altered volcanic clasts of reddish-brown colour (Fig. 14) and fresh phenocrysts of Px and Amp (Fig. 6h), inside the overlying chaotic conglomerate (1046–1051 m), indicated short transport by gravity flow mechanism. Admixture of new cummingtonite-bearing volcanic lithoclasts indicate deposition connected with the 4th stage of the Štiavnica stratovolcano (Šarinová & Rybár 2018). However, volcanic conglomerates, sandstones, bentonite and other clasts of volcanic origin clearly confirm the dominance of volcanic provenance. From the point of view of provenance, it is interesting, that rhyolite material and spherulites, which occur abundantly in the VR-1 well, are not observed in the ZM-1 well. This fact points to two separate source areas; first for the vicinity of the ZM-1 and second for the vicinity of the VR-1, both coming from the NE. Rhyolite and spherulite clasts, which significantly dominated in the depth of 2207–2104 m in the VR-1 well, can be derived from the Jastrabá Fm. The closest outcrops of the Jastrabá Fm. are situated to the NE of Nová Baňa town (Fig. 1). This provenance is supported by similar composition of Pl phenocrysts from the VR-1 well (Table 3) and rhyolites from the Jastrabá Fm. (Demko 2010). Additionally, the presence of rhyolite conglomerate near Tekovské Nemce village confirms transport from this area. At the depth of 2055 m, a rapid change to andesite character of volcanic debris is observed. This fact can be interpreted in two ways: 1) by deep erosion, which started by removal of the Jastrabá Fm. and continued to erode the relatively older Priesil and Inovec Fm., or 2) by onset of andesite volcanic activity during the transportation of rhyolite epiclasts. The second option is in contradiction with the evolutionary stages of the Štiavnica Stratovolcano (Konečný et al. 1998; Chernyshev et al. 2013), but the new ages of the Jastrabá Fm. from Nová Baňa town (12.31–12.03 Ma by Lexa & Pécskay 2010) and the Priesil to Inovec fms. (13–12.2 Ma by Chernyshev et al. 2013) allow us to think in this direction. This possibility is supported by the absence of andesite clasts in rhyolite sandstones and conglomerates just as in the base of the rhyolite interval. However, this can be explained by the incompleteness of the well core material or by river avulsion.

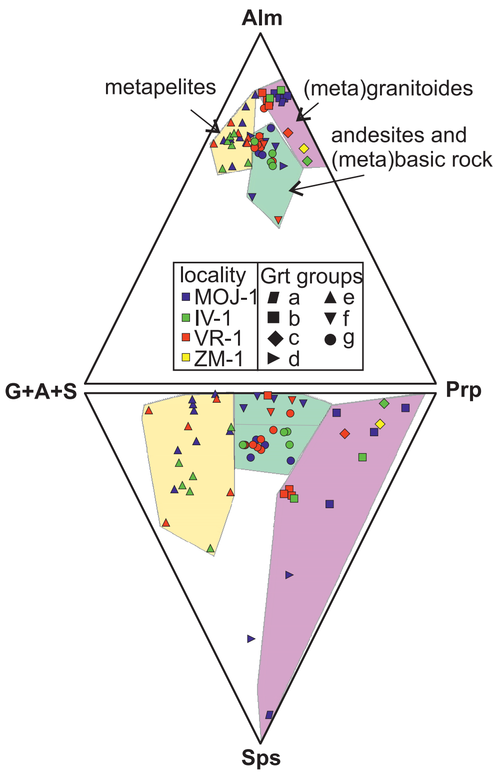

Fig. 15. Garnet provenance diagram after Suggate & Hall (2014; G+A+S=Grossular+Andradite+Schorlomite): **a–c** — origin in granitoide to gneiss: a — granite, b — low Mg gneiss, c — Mg-rich metapelite or gneiss; **d** — ?Bt-paragneiss; **e** — low grade metapelites (mica schist) to amphibolites; **f, g** — intermediate to basic rocks: f — ?metabasite, g — andesite.

In the upper part of the VR–1 well, the content of the stable material increases upward. Admixture of altered andesite and rhyolite lithoclasts, including the idiomorphic quartz crystals, points to recycling of older deposits. Also, less abundant sandstone clasts can be explained by recycling of the older fill, although the presence of mica with St and Cld intergrowths (Fig. 12) indicate the first cycle of erosion of mica-schists. This can be explained by the continued erosion of the basement rock in the volcanic field. In contrast to previous wells, the presence of the volcanic source in fine-grained, heterolithic sediments of the IV-1 well is documented only by $Grs_{9-24}Prp_{10-21}Alm_{59-69}$ garnets (Fig. 15) and by rare volcanic clasts (1760 m).

In the upper part of the wells (Pannonian/Tortonian–Messianian age), the amount of material derived from cover and nappe units, as well as from the Neogene volcanics decreases. On the other hand, the amount of clasts derived from granitoids increases. The composition of the clast in the ZM-1, MOJ-1 and IV-1 wells corresponds to the adjacent parts of the Tribeč Mts. Admixture of well-rounded volcanic lithoclasts in the ZM-1 well and altered Neogene volcanic clasts in the IV-1 well indicated continual but already less significant volcanic provenance and a relatively long transport. The para-conglomerate from the Serravallian–Pannonian boundary with well-rounded clasts indicates reworking of underlying sediments. This is manifested by: 1) composition similarity; 2) presence of intraclasts; 3) presence of chloritized Bt which was derived from underlying volcanic-rich sediments (ZM-1); 4) high content of ferric oxide in the heavy fraction (IV-1) as well as 5) by the presence of Sarmatian (late Serravalian) allochthonous nanofossils (IV-1, VR-1, ZM-1). The fine-grained development of the VR-1 well does not allow comments on the evolution of provenance in the central part of Komjatice depression.

The composition of the heavy minerals corresponds to the stated provenance, where the presence of St, Cld, Sil, Tur, $Grs_{8-24}Alm_{52-83}$ and $Prp_{7-18}Sps_{29-40}Alm_{41-43}$ garnets indicate origin in the metasediments and Bt paragneiss of the Tribeč Mts. The tourmaline zonality from schorl core to dravite rim (Fe/Fe+Mg=0.63–0.26), found in the MOJ-1 well, is opposite to the zonality described in tourmaline rich horizons from the Lúžna Fm. of the Tribeč Mts. (Vozárová et al. 2003). Schorl component increases towards the rim (Fe/Fe+Mg= 0.14–0.23) in dravite laminas from the basement rocks of the IV-1 well, just as in the Lúžna Fm. Identical zonality as in the MOJ-1 well is found in a Tur from schist lithoclast found in the ZM-1 well (Table 2; Fig. 12). This excludes Tur provenance from the Lúžna Fm. and confirms transport from the NE. $Alm_{24}Sps_{65}$ (MOJ-1 well) and $Prp_{11-21}Alm_{69-82}$ garnets (MOJ-1, IV-1 and VR-1 wells) together with schorls (Fe/Fe+Mg= 0.92–0.94; IV-1) correspond to granitoid provenance. Occurrence of magnesio-chromite in the heavy fraction of the IV-1 well points to recycling of the lower part of the Neogene fill, which contains melaphyre clasts. $Grs_{9-24}Prp_{10-21}Alm_{59-69}$ garnet probably derived from Neogene volcanic rocks reach the MOJ-1 well and confirm the existing transport direction from the NE. The presence of rare Hbl in the MOJ-1 well can be derived from granitoid rocks, but Hbl of similar composition is found in Neogene volcanic-rich horizons of the ZM-1 well (Šarinová & Rybár 2018).

The Cretaceous, Paleogene and Badenian fossils (Kováč et al. 2006, 2008; Ozdínová 2012; Zahradníková et al. 2013; our results) point to the presence of such sediments in the source area and/or their recycling. It is possible to speculate, that Badenian sediments were derived from the SE, for example, from the northern part of the Želiezovce depression (Kováč et al. 2018). The Cretaceous and Paleogene sediments may have formed the cover of the Central Western Carpathian units.

Stratigraphy

The original assignment of sediments based mainly on benthic foraminifera species as in Biela (1978a), is modified based on the new results from biostratigraphy and indirect dating of volcanic material. The assignment of formations is also affected by determination of the Nemčiňany Fm. and by genetic redefinition of the Pannonian (Tortonian–Messinian) sedimentary formations (Sztanó et al. 2016).

Several biostratigraphical markers are applied from the presented foraminiferal assemblages: the late Badenian (early Serravallian) *Bogdanowiczia pocutica*; the Sarmatian (late Serravallian) *Elphidium hauerinum* (Fig. 2)*, Nonion biporus* and also *Anomalinoides dividens* acme; and the Pannonian ?*Trochammina kibleri* (Fig. 2). Recorded nannofossil markers are: the Sarmatian association with *Calcidiscus pataecus* (*sensu* Schütz et al. 2007; Galović & Young 2012; Galović 2017; Fig. 3), *Calcidiscus tropicus* acme (Fig. 3) together with rare specimens of *Calcidiscus macintyrei*; and the Pannonian *Isolithus semenenko* and *Reticulofenestra tegulata* (Fig. 3). The dinocysts *Virgodinium asymmetricum, V. transformis, Spiniferites bentori pannonicus, S. bentori oblongus, Pontiadinium pecsvaradensis, P. obesum* assigned to the Spiniferites bentori oblongus Zone (Sütő-Szentai 1988) are used for the verification of the early Pannonian (Tortonian) age. This is the most diverse and rich assemblage calibrated with Biochron ~10.8 Ma (Magyar et al. 1999a), Congeria banatica–Lymnocardium gorjanovici–Gyraulus tenuistriatus Cenozone (Vrsaljko 1999) and NN9a-b to NN9b Zone (Bakrač et al. 2012).

Upper Badenian–Sarmatian (Serravallian)

The presence of *Bogdanowiczia pocutica* in the lowermost part of the MOJ-1 well (2100–2095 m) indicates late Badenian (early Serravallian) age. The pre-tectonic age of these sediments is supported by the presence of veins cutting through mineral grains in the depth of 2046–2050 m (Fig. 6). The Sarmatian (late Serravallian) age of the following heterolithic sediments (2010–1795 m) is documented by the presence of algae *Halicoryne* aff. *morelleti* and *Elphidium hauerinum* with FO in the upper part of the early Sarmatian (*sensu* Piller & Harzhauser 2005) in the Paratethys (Cicha et al. 1998). These results are consistent with Biela (1978a) and the strata can be assigned to the Vráble Fm. The following coarse-grained interval from the Sarmatian–Pannonian boundary was originally assigned to the Sarmatian (Biela 1978a). The newly defined, coarse-grained marginal Nemčiňany Fm. (Sztanó et al. 2016) corresponds to these sediments much better.

The Sarmatian (late Serravallian) age of the basal sediments from the IV-1 well (2355–1950 m; Biela 1978a) is supported by the presence of a poor nannofossil assemblage (2315 m) including *Cyclicargolithus floridanus.* Its last common occurrence can be found at the NN6/NN7 (Martini 1971) zones boundary. A clear stratigraphic assignment of these deposits comes from heterolithic sediments that overlie the coarse clastics of the IV-1 well (Figs. 7, 8). Here the NN6 was recognized in the depth of 2090–2093 m (Zahradníková et al. 2013). Moreover, the Sarmatian age of these sediments is supported by the presence of *Halicoryne* aff. *morelleti* and *Elphidium hauerinum* (2093–2040 m), as well as by *Bolivina sarmatica* in the depth of 1961–1956 m.

In the case of the VR-1 well, non-volcanic conglomerate from the base of the Neogene fill was originally assigned to the middle Badenian (Langhian), while volcanic conglomerates and sandstones were assigned to the late Badenian (Serravallian; Biela 1978a). These assignments were based on benthic foraminiferal assemblages in the overlaying sediments. In this study, the first abundant, but poorly preserved marine nannofossils and dinocyst ?*Cleistosphaeridinium placacanthum* from the depth of 1801–1804 m indicates late Badenian–Sarmatian (Serravallian) age. The Sarmatian age (NN6; 1750–1203 m), has been set based on a small *Calcidiscus* resembling *C. pataecus*? and higher numbers of *Calcidiscus* species starting to appear in the depth of 1745–1750 m including the *C. tropicus* acme (1203 m; Suppl. 1). Within the foraminifera assemblage the *Anomalinoides dividens* acme (1745–1750 m), indicates the base of marine Sarmatian sediments. Occurrence of *Nonion biporus* with *Elphidium hauerinum* (up to 1250 m) supported this assignment. However, biostratigraphic sterility of underlying sediments (~1850 m–2300 m) can be explained by the dominance of coarse-grained volcanic material. In addition, the present volcanic material indicates Sarmatian age. Rhyolite clasts which appear from the depth of 2207 m (Figs. 6, 10) can be linked to the Jastrabá Fm. outcropping NE of Nová Baňa town (Fig. 1). This interpretation is suggested by the presence of the rhyolite conglomerate occurring near Tekovské Nemce village. Original dating of rhyolites in the vicinity of Nová Baňa town yield a cooling age of 14.4±0.5 Ma from Bt and 13.8±0.3 Ma from volcanic glass (Repčok 1981 in Konečný et al. 1998). New K/Ar dating of rhyolites from the vicinity of Nová Baňa yield an age of 12.31±0.44–12.03±0.38 Ma, with a mean of 12.19 Ma (Lexa & Pécskay 2010). Nevertheless, the latest K/Ar and Rb/Sr dating for the whole Jastrabá Fm. is in the interval between 12.2 ± 0.8 and 11.4 ± 0.4 Ma (Chernyshev et al. 2013). Additionally, the Sarmatian (late Serravallian) age of these sediments is supported by the high content of andesitic material in the overlaying sediments (2055 m and above). In this depression, andesites of the 4th stage of the Štiavnica stratovolcano (especially Priesil Fm.) formed an elevation on the surface. In the past, the Priesil and Inovec Fm. were assigned to the late Badenian–Sarmatian (intra Serravallian) boundary (Konečný et al. 1998). The new absolute dating by K/Ar and Rb/Sr indicates an age of 13–12.2 Ma (Chernyshev et al. 2013), although the authors discussed age ranges from 12.7 to 12.2 Ma. The age limits of both Jastrabá and Priesil fms. do not contradict the observed sedimentary record and indicated a Sarmatian (late Serravallian) age of these deposits. Presence of poorly preserved nannofossils indicating late Badenian age (1801–1804 m), can be explained by recycling of older strata during opening of the depression accompanied by volcanic activity. The sandy, gravity flow character of the deposits connected with rapid sedimentation, tectonic activity and volcanism supports this fact. According to this point of view, the non-volcanic conglomerates from the basal part of the Neogene fill are older than 12.2 Ma.

The base of the Neogene fill in the ZM-1 well is questionable and cannot be commented because of lack of core samples. The question about the assignment of the non-metamorphosed sandstones from the interval 1904–1804 m remains. Gaža & Beinhauerová (1976) assign these rocks to the Carboniferous and Biela (1978a) describes a core fragment from a depth of 1900 m as a possible Pre-Cenozoic rock. The following ochre and brick-red coloured arkosic sandstones (1590 m), which were marked as Permian (Gaža & Beinhauerová 1976) were not found in the repository. However, based on presence of the mottled mudstones (Fig. 11) and other structures typical for an alluvial environment (1553–1558 m) it is likely, that the colouring was caused by pedogenesis, and not by Permian arid deposition. The presence of micritic carbonate clasts (1711 m) is also not typical for the composition of the Permian sediments of the Hronic unit (Vozárová & Vozár 1988). As suggested by Biela (1978a), similar lithological composition of samples from the depth of 1711–1448 m supports this view and points to the Neogene age. However, these sediments are biostratigraphically barren. A Cenozoic age is indicated by a poor nannofossil assemblage (1555–1551 m). Although the first foraminifera tests are observed in the depth of 1405–1410 m, biostratigrafical markers such as *Nonion communis, Bulimina elongata* and *Uvigerina semiornata* are present no sooner than at the depth of 1351 m. Extremely high content of pyrite and molds with small remains of dissolute, calcareous tests indicate that the assemblage represents only a fraction of the original association. According to the present foraminifera markers in the upper parts of the well, a late Badenian association typical for "agglutinated zone" is assumed. The dinocysts *Melitasphaeridium choanophorum* and *Cleistosphaeridinium placacanthum* from this depth (1351 m) can be correlated with the NN6 Zone. Dominance of *Bolivina dilatata maxima* (1258–1046 m) is typical for the late Badenian. However, fragmented tests, signs of dissolution (1255 m, 1051 m) and size sorting of smaller forams suggest reworking from the older late Badenian strata. Presence of the NN6 Zone in the depth of 400–1200 m was first mentioned by Ozdínová (2012). This is consistent with the presented results, where calcareous nannofossils showed the NN6 Zone (1351–1201 m). Late Badenian affinity is based on the common *Calcidiscus* *premacintyrei*, *Helicosphaera walbersdorfensis*, *H. wallichii*, *Sphenolithus abies*, *Reticulofenestra pseudoumbilicus*, *Umbilicosphaera rotula*, *Holodiscolithus macroporus*, *Braarudosphaera bigelowii bigelowii* (Suppl. 1). Numerous poorly preserved *Calcidiscus* in the depth of 1051–1046 m indicate a Sarmatian age. Redeposition of fossil assemblages is supported by observed slump structures and intraclasts (1051–1000 m; Fig. 11). Apart from biostratigraphy, indirect dating of volcanic material was possible. Based on the texture and mineral composition, the Bt–Amp±Px andesite to dacite from coarse-grained conglomerates (1350 and 1100 m) is assigned to the Studenec Fm. (Figs. 6, 11). Original dating of the Studenec Fm. by K/Ar method was set to 15.2±0.1 Ma (Konečný et al. 1969 in Konečný et al. 1998) and by the FTA method to 14.8–16.4 Ma (Repčok 1978, 1979, 1980, 1981 all in Konečný et al. 1998). These ages did not line up with biostratigraphy (Konečný et al. 1998). Nonetheless, the new K/Ar and Rb/Sr data yield an age of 13.1±0.3 Ma to 12.4±0.1 Ma (Chernyshev et al. 2013); although the authors discuss an age range of 13.1–12.7 Ma. In the ZM-1 well, only the altered, rusty-brown volcanic lithoclasts from the chaotic conglomerate (1051–1005 m) can be assigned to the 4th stage of the Štiavnica stratovolcano evolution (Šarinová & Rybár 2018; Figs. 6, 11) with an age of 12.7–12.2 Ma (Chernyshev et al. 2013). Based on the above mentioned information, the late Badenian–Sarmatian (Serravallian) age of this volcanosedimentary interval can be considered, in contrast to the original assignment (Gaža & Beinhauerová 1976; Biela 1978a). Nonvolcanic terrestrial sediments from the basal part are older than 12.7 Ma.

The actual stratigraphy (Vass 2002) assigned the late Badenian (early Serravallian) sediments to the Pozba Fm. and Sarmatian (late Serravalian) sediments to the Vráble Fm., both with littoral to shelf character. The formations defined based on their age are difficult to use, especially when the NN6 Zone is typical for both formations. In addition, environments are normally time transgressive, therefore genetically-defined formations are more suitable for interpretations. Because of the impossibility of the strict separation of the marine sediments into the Pozba and Vráble formations, they are included in the merged Vráble–Pozba Fm. (Fig. 16). The actual definition (Vass 2002) does not include the underlying alluvial sediments. For the alluvial to fluvial sediments a new formation is defined, with the name adopted from the stratotype section in the Zlate Moravce-1 well = Zlaté Moravce Formation.

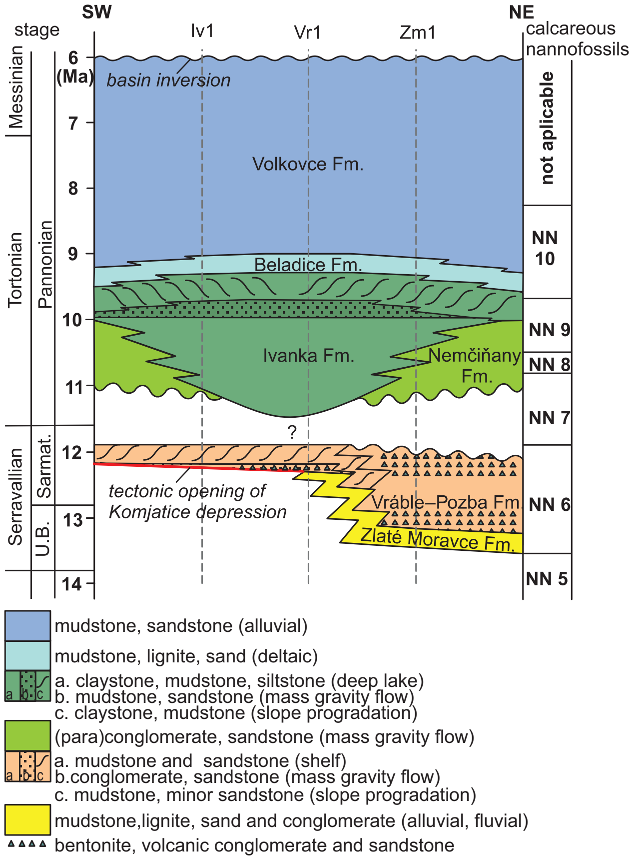

Fig. 16. Lithostratigraphy of the Komjatice depression.

The Zlaté Moravce Formation

Lithology, facies: The Zlaté Moravce Fm. is dominantly built up by grey mudstones, which are cut and filled by light coloured conglomerates and sandstones. Red mottles, synsedimentary folds, and carbonized plant fragments are common (Fig. 14). Muddy horizons with red mottles and abundant carbonized plant fragments are interpreted as swamps or oxbow lakes. Polymict conglomerate and sandstone are fine-grained, poorly rounded and composed mainly of Qz-, Qz-sericitic and carbonate shale lithoclasts. Altered granitoids to meta-granitoids meta-greywacke, meta-arkose, chert/felsite, quartz arenite, arkose, wacke, carbonates, Fsp, Bt and rare melaphyre are also included. In the upper part, Neogene volcanic lithoclasts start to appear. Presence of normal gradation, imbrications and erosive surfaces points to deposition by traction currents. These features clearly coincide with an alluvial environment, which is partly supported by the cyclic character of the well logs (Fig. 13).

Stratigraphic position, thickness: The thickness is more than 270 m in the ZM-1 well and 160 m in the VR-1 well (depth 2300–2454 m). The formation overlies pre Cenozoic basement and passes into the marine Vráble-Pozba Fm. of late Badenian–Sarmatian (Serravalian) age.

Fossils, age: The sediments are biostratigraphically barren. The assumed age is Serravallian which is derived from the correlation with the syn-rift packet defined on the seismic lines 3/99 (Šályová & Mojžiš 2002) and 820/00 (provided by Equis l.t.d).

Depositional environments: The Zlaté Moravce Fm. represents terrestrial sediment which was deposited on an alluvial fan. These sediments continually pass into a fan delta environment belonging to the Vráble–Pozba Fm., what is documented by marine fossils. In this context, the Zlaté Moravce Fm. represents a proximal facies of the newly opened depocenters (Komjatice, ?Rišňovce, ?Gabčíkovo depressions).

Representative outcrops and wells: The stratotype section can be found in the ZM-1 well (1440–1711 m). The material can be found in the repository of Nafta a.s. in Gbely town. This formation is also recognized in the basal part of the VR-1 well, but unfortunately no core material is available in the repository today.

Pannonian (Tortonian–Messinian)

The Pannonian (Tortonian–Messinian) age of the sedimentary record was originally recognized by Biela (1978a). This study refines the conclusion based on the Pannonian (Tortonian) *Reticulofenestra tegulata* (1603–1612 m in IV-1; 1005–1010 m in ZM-1) and *Isolithus semenenko* acme together with the lowermost occurrence acme of ?*Trochammina kibleri* (1154 m of VR-1 well). The acme of *Reticulofenestra tegulata* in the ZM-1 well is in contradiction with the original, Sarmatian age (Biela 1978a). In this case, a younger, Pannonian age is also supported by an erosional unconformity, significant change in provenance and by a high degree of weathering. Pannonian dinoflagellates are present in the ZM-1 (658–551 m), IV-1 (up from 1763 m) and VR-1 wells (up from 1050 m). In the VR-1 well, a dinoflagellate association can be correlated with the NN9ab–NN9b Zone (755–603 m; Suppl. 1). This age range is consistent with a 9.62±0.57 to 9.14±0.57 Ma age based on $^{10}Be/^{9}Be$ dating from overlying sediments (555–505 m; Šujan et al. 2016).

The new assignment of the formations is affected by introduction of the Nemčiňany Fm. and by genetic redefinition of the Pannonian (Tortonian–Messinian) sedimentary formations (Sztanó et al. 2016; Fig. 16). The Nemčiňany Fm. is defined as basal, coarse-grained braided river to fan delta deposits representing pre-trangressive facies in marginal parts of Lake Pannon. In the studied wells, the para-conglomerate and other coarse-grained sediments from the Sarmatian–Pannonian (Serravallian–Tortonian) boundary are assigned to the Nemčiňany Fm. (Figs. 4, 7, 13, 16). In the past, these sediments were often assigned to the upper part of the Vráble Fm. (MOJ-1, ZM-1; Biela 1978a). It was caused by recycling or by fossil sterility of the coarse-grained sediments, as well as by an incorrect division of the underlying, volcanic sediments (ZM-1). The time span of the Nemčiňany Fm. was determined by $^{10}Be/^{9}Be$ dating from the Nemčiňany outcrop in the time span of 11.72±0.88 to 11.21±1.23 Ma and from the ŠVM-1 well (Fig. 1) in the time span of 11.23±0.84 to 9.92±0.63 Ma (Šujan et al. 2016). In the central part of the depression (VR-1) the Nemčiňany Fm. is not present, but the Sarmatian–Pannonian (Serravallian–Tortonian) boundary (1208–1149 m) is characterized by well preserved pollen and no dinocysts, which indicates marginal conditions. Only the brackish lacustrine sediments without presence of terrestrial facies are assigned to the Ivanka Fm. (Sztanó et al. 2016). This environment is supported by *Isolithus semenenko* acme, as well as by the dinoflagellate assemblages. Additional evidence comes from prevailing fine-grained lithology and from prograding clinoforms observed on the reflection seismic lines 3/99 (Šályová & Mojžiš 2002) and 820/00 (provided by Equis l.t.d). The change in grain size, which is also reflected in the SP and RT log, indicates a change in deposition. At this boundary, the deltaic deposition of the Beladice Fm. (Sztanó et al. 2016) begins.

Discussion

The older interpretation of this area considered a wide age range of the sedimentary fill (from middle Badenian to Sarmatian/Langhian–Serravalian; Gaža & Beinhauerová 1976; Biela 1978a; Hók et al. 1999 and others). The new indirect age data based on volcanic material are inconsistent with older interpretations. The new assignment is consistent with biostratigraphy, if it is noted that the coarse grained gravity flow character of deposits caused biostratigraphic sterility or reworking of fossils. According to Hók et al. (1999) the late Badenian to Sarmatian (Serravallian) sediments belong to one depositional event, with continual transition from terrestrial to marine environment (ZM-1, Vr-1 wells). The same facies are older in the NE and younger in the SW, which is supported by the presented provenance and biostratigraphic analysis. Presence of late Badenian (early Serravallian) sediments in the E (SE) can be explained by gradual tectonic opening of the depression. In the late Badenian, the Komjatice depression was not yet open. The deposition in the study area was probably connected to the margin of the older Želiezovce depression. The main phase of the deposition is associated with opening of the depression in simple shear tectonic regime (Hók et al. 2016). This led to the widening and deepening of the depositional environment followed by rapid deposition. Moreover, the syn-rift cycle is nicely observed on the reflection seismic line 820/00, which cuts through the VR-1 and seismic line 3/99 (Šályová & Mojžiš 2002). Since the extent of the Sarmatian (Serravallian) sediments is limited by the Mojmírovce fault system (Biela 1978a; Hók et al. 1999), the sea level did not reach the top of the footwall. The total thickness of the Sarmatian (Serravallian) sediments in the central part of the depression reaches more than 1100 m (VR-1). It is similar to the thickness of the Sarmatian sediments in the adjacent Rišňovce depression (Fordinál & Elečko 2000). In contrast, the Želiezovce depression contains lower Badenian (Langhian) sediments and only a low thickness of late Badenian–Sarmatian (Serravallian) deposits (e.g., Kováč et al. 2018).

The Sarmatian–Pannonian (Serravallian–Tortonian) boundary is erosive. The increase of water level during the Pannonian (Tortonian) is manifested by the deposition of coarse clastics of the Nemčiňany Fm. in marginal parts of the depression (Fig. 16). The deepwater environment of the Ivanka Fm. was sustained by further tectonic subsidence on the Mojmírovce Fault system (e.g., Gaža & Beinhauerová 1976; Hók et al. 1999). The cessation of the water level rise led to a gradual filling up of the depression (Fig. 16). The sedimentation of the deltaic Beladice Fm. and alluvial Volkovce Fm. followed (Fig. 16). The widespread Pannonian sediments are no longer limited by the Mojmírovce fault system (Biela 1978a; Hók et al. 1999).

Conclusion

Combination of new results from biostratigraphy and indirect dating of volcanic material brought changes to the assignment of the sedimentary record especially in the VR-1 and ZM-1 wells. In contrast to previous studies (Gaža & Beinhauerová 1976; Biela 1978a; Harčár et al. 1988; Hók 1999; Vass 2002) and in agreement with Szatnó et al. (2016) the formations are defined by their genetic origin. The new stratigraphic assignment of the Komjatice depression can be defined as follows (Fig. 16):

- Zlaté Moravce Fm.: a newly defined formation containing alluvial deposits. The late Badenian–Sarmatian (Serravalian) age is set based on its stratigraphic position. The Zlaté Moravce Fm. represents the base of sedimentary fill linked to initial opening of the depression.
- Vráble–Pozba Fm.: Late Badenian–Sarmatian (Serravalian) age is documented by biostratigraphical markers and by indirect dating of volcanic rocks. The deposition of marine sediments is connected with the tectonic opening of the depression.
- Nemčiňany Fm.: contains coarse-grained sediments from the Sarmatian–Pannonian (Tortonian–Serravallian) boundary. The most visible trend of erosion and recycling is observed in the eastern part of the depression (ZM-1 well).
- The following Pannonian (Tortonian–Messinian) formations are divided based on their lithology, fossil assemblages, well log patterns and seismic reflection character into: the predominantly fine-grained Ivanka Fm. (basin floor to slope); the sandy deltaic Beladice Fm., and the predominantly muddy, alluvial Volkovce Fm.

The main transport direction in the late Badenian–Sarmatian (Serravallian) time was from the NE to SW and the provenance area contained Paleozoic rocks from the Hronic unit and subsequently also Neogene volcanic rocks. The length of transport was short in the eastern part and increased towards the west. During the Pannonian (Tortonian–Messinian) time, the main provenance area was located in the Tribeč Mts., although the direction of transport from the E remained.

Acknowlegements: This research was supported by the Slovak research and development agency under the contracts No. APVV-16-0121, APVV-0099-11, APVV-15-0575 & APVV-14-0118. The authors wish to express their gratitude to the Management of Nafta petroleum company and to Dr. Sliva for allowing access to the well-core repository; to the Equis ltd. for providing data (seismic line 820/00); to Dr. Bakrač and Dr. Soliman for dinoflagellate taxonomy discussion; Dr. Teodoridis for leaf taxonomy discussion; and to Dr. Kostič for assistance with the QUANTA FEG 250. We express our gratitude to the editor and to the reviewers for their insightful comments which improved the manuscript.

Reference

Bakrač K., Koch G. & Sremac J. 2012: Middle and Late Miocene palynological biozonation of the south-western part of Central Paratethys (Croatia). *Geologica Croatica* 65, 2, 207–222.

Biela A. 1978a: Deep wells in the covered regions of inner Western Carpathians. *Regional geology of Western Carpathians* 10, 1–224 (in Slovak).

Biela A. 1978b: Deep wells in the covered regions of inner Western Carpathians II. *Regional geology of Western Carpathians* 10, 1–224 (in Slovak).

Boggs Jr. S. 2006: Principles of Sedimentology and Stratigraphy. Fourth ed. *Pearson Prentice Hall*, Upper Saddle River, 1–662.

Bóna J. & Gál M. 1985: Kalkiges nannoplankton im Pannonien Ungarns. In: Papp A. (Ed.): Chronostratigraphie und Neostratotypen Miozän der Zentralen Paratethys, 7, M6 Pannonien. *Akademia Kiadó*, Budapest, 482–515.

Chalupová B. 2006: Paleoecology of the Sarmatian fish fauna in the Danube basin (Slovakia). *Mineralia Slovaca* 38, 4, 321–326 (in Slovak).

Chernyshev I.V., Konečný V., Lexa J., Kovalenker V.A., Jeleň S., Lebedev V.A. & Goltsman Y.V. 2013: K–Ar and Rb–Sr geochronology and evolution of the Štiavnica Stratovolcano (Central Slovakia). *Geol. Carpath.* 64, 4, 327–351.

Cicha I., Rögl F., Rupp Ch. & Čtyroká J. (Eds.) 1998: Oligocene–Miocene foraminifera of the Central Paratethys. *Abhandlungen der Senckenbergischen Naturforschenden Gesellschaft* 549, 1–325.

Ćorić S. & Gross M. 2004: Kalkiges Nannoplankton aus dem Unter-Pannonium des Oststeirischen Beckens (Österreich). *Joannea Geologie und Paläontologie* 5, 9–18 (in German with English abstract).

Čermák D. 1972: Lithological description of mechanical drill cores sampled at the Ivánka-1 well, near Nitra town. *Open file report, Manuscript archive Nafta a.s. Plavecký Štvrtok*, 1–8 (in Slovak).

Čermák D. 1976a: Final geological report from the Ivánka-3 well. *Open file report, Manuscript archive Nafta a.s. Plavecký Štvrtok*, 1–16 (in Slovak).

Čermák D. 1976b: Final geological report from the Ivánka-5 well. *Open file report, Manuscript archive Nafta a.s. Plavecký Štvrtok*, 1–15 (in Slovak).

Čermák D. 1976c: Final geological report from the Ivánka-6 well. *Open file report, Manuscript archive Nafta a.s. Plavecký Štvrtok*, 1–23 (in Slovak).

Čermák D. 1977a: Final geological report from the Ivánka-4 well. *Open file report, Manuscript archive Nafta a.s. Plavecký Štvrtok*, 1–14 (in Slovak).

Čermák D. 1977b: Final geological report from the Ivánka-7 well. *Open file report, Manuscript archive Nafta a.s. Plavecký Štvrtok*, 1–14 (in Slovak).

Čermák D. 1977c: Final geological report from the Ivánka-8 well. *Open file report, Manuscript archive Nafta a.s. Plavecký Štvrtok*, 1–12 (in Slovak).

Demko R. (Ed). Lexa J., Koděra P., Biroň A., Smolka J., Šesták P., Konečný P., Tuček Ľ., Ferenc Š., Bačo P., Repčiak M., Kollárová V., Pipík Kiška R., Mikušová J., Kotulová J., Bystrická G. & Vlachovič J. 2010: Paleovolcanic reconstruction maps of rhyolite volcanics of Slovakia an analysis of magmatic and hydrotermal preoceses. Final report of the geological task 15 06. *Open file report, Geofond*, Bratislava, 1–728 (in Slovak).

Fordinál K. & Elečko M. 2000: Ripňany Formation–a Sarmatian and Early Pannonian fresh water sedimentary assemblage of the Rišňovce depression. *Mineralia Slovaca* 32, 55–60.

Fusán O., Biely A., Ibrmajer J., Plančár J. & Rozložník L. 1987a: Basement of the Tertiaty of the Inner West Carpathians. *GÚDŠ*, 1–123.

Fusán O., Plančár J. & Ibrmajer J. 1987b: Tectonic map of Basement of Tertiary in Inner West Carpathians. *GÚDŠ*, Bratislava.

Galović I. 2017: Sarmatian calcareous nannofossil assemblages in the SW Paratethyan marginal marine environments: Implications for palaeoceanography and the palaeoclimate. *Progress in Oceanography* 156, 209–220.

Galović I. & Young J. 2012: Revised taxonomy and stratigraphy of Middle Miocene calcareous nannofossils of the Paratethys. *Micropaleontology* 58, 4, 305–334.

Gaža B. 1968: Final geological report from the structural well Vráble-l. *Open file report, Manuscript archive Nafta a.s. Plavecký Štvrtok*, 1–11 (in Slovak).

Gaža B. 1970: Final geological report from the structural well Zlaté Moravce-1. *Open file report, Manuscript archive Nafta a.s. Plavecký Štvrtok*, 1–11 (in Slovak).

Gaža B. 1975: Final geological report from the Ivánka-2 well. *Open file report, Manuscript archive Nafta a.s. Plavecký Štvrtok*, 1–19 (in Slovak).

Gaža B. 1977: Final geological report from the Ivánka-9 well. *Open file report, Manuscript archive Nafta a.s. Plavecký Štvrtok*, 1–8 (in Slovak).

Gaža B. & Beinhauerová M. 1976: On the geology of the Zlaté Moravce bay (Danube basin), *Mineralia Slovaca* 8, 3, 221–240 (in Slovak with English summary).

Harčár J. & Priechodská Z. (Eds.), Karolus K., Karolusová E., Remšík A. & Šucha P. 1988: Explanations to the geological map of the North-Eastern part of the Podunajská Lowland 1:50,000. *GÚDŠ*, Bratislava, 1–114 (in Slovak with English summary).

Hók J., Kováč M., Kováč P., Nagy A. & Šujan M. 1999: Geology and tectonics of the NE part of Komjatice Depression. *Slovak Geological Magazine* 5, 3, 187–199.

Hók J., Kováč M., Pelech O., Pešková I., Vojtko R. & Králiková S. 2016: The Alpine tectonic evolution of the Danube Basin and its northern periphery (southwestern Slovakia). *Geol. Carpath.* 67, 5, 495–505.

Holbourn A., Kuhnt W., Clemens S., Prell W. & Andersen N. 2013: Middle to late Miocene stepwise climate cooling: Evidence from a high-resolution deep water isotope curve spanning 8 million years. *Paleoceanography* 28, 688–699.

Ivanička J. (Ed.)., Hók J., Polák M., Határ J., Vozár J., Nagy A., Fordinál K., Pristaš J., Konečný V., Šimon L., Kováčik M., Vozárová A., Fejdiová O., Marcin D., Liščák P., Macko A., Lanc J., Šantavý J. & Szalaiová V. 1998: Explanations to the geological map of Tribeč Mts, 1:50,000. *GÚDŠ*, Bratislava, 1–246 (in Slovak with English summary).

Káčer Š. (Ed.), Polák M., Bezák V., Hók J., Teťák F., Konečný V., Kučera M., Žec B., Elečko M., Hraško Ľ., Kováčik M., Pristaš J., Káčer Š., Antalík M., Lexa J., Zvara I., Fritzman R., Vlachovič J., Bystrická G., Brodianska M., Potfaj M., Madarás J., Nagy A., Maglay J., Ivanička J., Gross P., Rakús M., Vozárová A., Buček S., Boorová D., Šimon L. & Mello J. 2013: Slovak Republic — digital geological map in scale of: 1:50,000 and 1:500,000. *GÚDŠ*, available at http://apl.geology.sk/gm50js.

Konečný V. (Ed.), Lexa J., Halouzka R., Hók J., Vozár J., Dublan L., Nagy A., Šimon L., Havrila M., Ivanička J., Hojstrovičová V., Miháliková A., Vozárová A., Konečný P., Kováčikova M., Filo M., Marcin D., Klukanová A., Liščák P. & Žáková E. 1998: Explanations to the geological map of Štiavnica Mts. and Pohronský Inovec Mts. (Štiavnica stratovolcano). *GÚDŠ*, Bratislava, 1–473 (in Slovak with English summary).

Kováč M., Baráth I., Fordinál K., Grigorovich A. S., Halásová E., Hudáčková N., Joniak P., Sabol M., Slamková M., Sliva Ľ. & Vojtko R. 2006: Late Miocene to Early Pliocene sedimentary environments and climatic changes in the Alpine–Carpathian–Pannonian junction area: A case study from the Danube Basin northern margin (Slovakia). *Palaeogeogr. Palaeoclimatol. Palaeoecol.* 238, 32–52.

Kováč M., Andrejeva-Grigorovič A., Baráth I., Beláčková K., Fordinál K., Halásová E., Hók J., Hudáčková N., Chalupová B., Kováčová M., Sliva Ľ. & Šujan M. 2008: Lithological, sedimentological and biostratigraphical evaluation of the ŠVM-1 Tajná well. *Geologické práce, Správy* 114, 51–84 (in Slovak with English abstract).

Kováč M., Synak R., Fordinál K. & Joniak P. 2010: Dominant events in the northern Danube Basin palaeography — a tool for specification of the Upper Miocene and Pliocene stratigraphy. *Acta Geologica Slovaca* 2, 1, 23–36.

Kováč M., Synak R., Fordinál K., Joniak P., Tóth C., Vojtko R., Nagy A., Baráth I., Maglay J. & Minár J. 2011: Late Miocene and Pliocene history of the Danube Basin: inferred from development of depositional systems and timing of sedimentary facies changes. *Geol. Carpath.* 62, 6, 519–534.

Kováč M., Rybár S., Halásová E., Hudáčková N., Šarinová K., Šujan M., Baranyi V., Kováčová M., Ruman A., Klučiar T. & Zlinská A. 2018: Changes in Cenozoic depositional environment and sediment provenance in the Danube Basin. *Basin Research* 30, 97–131.

Lankreijer A., Kováč M., Cloethingh S., Pitoňák P., Hlôška M. & Biermann C. 1995: Quantitative subsidence analysis and forward modelling of the Vienna and Danube basins: thin-skinned versus thick-skinned extension. *Tectonophysics* 252, 433–451.

Lénárt R. & Hók J. 2013: Polyphase deformation of the cover sequence and granitic rocks of the Zobor part of the Tribeč Mts. *Acta Geologica Slovaca* 5, 1, 107–115.

Lentin J.K. & Williams G.L. 1998: Fossil dinoflagellates: index to genera and species. 1998 edition. *AASP, Contribution series* 34, 1–817.

Lexa J. & Pécskay Z. 2010: Radiometric dating of rhyolite of Jastrabá Fm. by conventional K/Ar method. In: Demko R. (Ed.). Lexa J., Koděra P., Biroň A., Smolka J., Šesták P., Konečný P., Tuček Ľ., Ferenc Š., Bačo P., Repčiak M., Kollárová V., Pipík Kiška R., Mikušová J., Kotulová J., Bystrická G. & Vlachovič J.: Paleovolcanic reconstruction maps of rhyolite volcanics of Slovakia an analysis of magmatic and hydrotermal preoceses. Final report of the geological task 15 06. *Open file report, Geofond*, Bratislava, 86–100 (in Slovak).

Locock A.J. 2008: An Excel spreadsheet to recast analyses of garnet into end-member components, and a synopsis of the crystal chemistry of natural silicate garnets. *Computers & Geosciences* 34, 1769–1780.

Loeblich A.R. & Tappan H. 1992: Present status of Foraminiferal Classification. In: Takayanagi Y. & Saito T (Eds.): Studies in Benthic Foraminifera. *Tokai University Press*, 93–102.

Łuczkowska E. 1974: Miliolidae (Foraminiferida) from the Miocene of Poland Part II. Biostratigraphy, palaeoecology, and systematics. *Acta Palaeontologica Polonica* 19, 1, 3–176.

Magyar I., Geary D., Sütő-Szentai M., Lantos M. & Müller P. 1999a: Integrated bio-, magneto and chronostratigraphic correlations of the Late Miocene lake Pannon deposits. *Acta Geologica Hungarica* 42, 1, 5–31.

Magyar I., Geary D.H. & Müller P. 1999b: Paleogeographic evolution of the Late Miocene Lake Pannon in Central Europe. *Palaeogeogr. Palaeoclimatol. Palaeoecol.* 147, 151–167.

Martini E. 1971: Standard Tertiary and Quaternary Calcareous Nannoplankton Zonation. In: Farinacci A. (Ed.): Proceedings of the II Planktonic Conference, Roma, 1970. *Edizioni Tecnoscienza*, 739–785.

Miall A.D. 2006: The geology of fluvial deposits. *Springer*, New York, 1–582.

Nichols G. 2009: Sedimentology and Stratigraphy. *Wiley-Blackwell*, Chichester, 1–419.

Ozdínová S. 2012: Redepositions of the Paleogene calcareous nannofossils in the Neogene sediments aroud the northern margin of the Danube Basin: The data source about uplift and erosion of the substrates. *Mineralia Slovaca* 44, 257–266 (in Slovak).

Piller W.E. & Harzhauser M. 2005: The myth of the brackish Sarmatian Sea. *Terra Nova* 17, 450–455.

Schütz K., Harzhauser M., Rögl F., Ćorić S. & Galović I. 2007: Foraminiferen und Phytoplankton aus dem unteren Sarmatium des südlichen Wiener Beckens (Petronell, Niederösterreich). *Jahrb. Geol. Bundesanst.* 147, 449–488.

Suggate S.M. & Hall R. 2014: Using detrital garnet compositions to determine provenance: a new compositional database and procedure. In: Scott R.A., Smyth H.R., Morton A.C. & Richardson N. (Eds.): Sediment Provenance Studies in Hydrocarbon Exploration and Production*. Geol. Soc. London, Spec. Publ.* 386, 373–393.

Sütő-Szentai M. 1988: Microplankton zones of organic skeleton in the Pannonian s.l. stratum complex and in the upper part of the Sarmatian strata. *Acta Botanica Hungarica* 34, 3–4, 339–356.

Sztanó O., Kováč M., Magyar I., Šujan M., Fodor L., Uhrin A., Rybár S., Csillag G. & Tőkés L. 2016: Late Miocene sedimentary record of the Danube/Kisalföld Basin: interregional correlation of depositional systems, stratigraphy and structural evolution. *Geol. Carpath.* 67, 6, 525–542.

Šályová B. & Mojžiš J. 2002: Ivanka pri Nitre-Golianovo locality calculation of gas reserves in an exclusive accumulation, state at 1st January 2002. *Open file report, Geofond*, Bratislava, 1–60+28 graph. attachments (in Slovak).

Šarinová K. & Rybár S. 2018: Cummingtonite-bearing volcanic rocks: first evidence in the Central Slovak Volcanic Field. *Geol. Carpath.* 69, 335–346.

Šujan M., Braucher R., Kováč M., Bourlés D. L., Rybár S., Guillou V. & Hudáčková N. 2016: Application of the authigenic $^{10}Be/^{9}Be$ dating method to Late Miocene–Pliocene sequences in the northern Danube Basin (Pannonian Basin System): Confirmation of heterochronous evolution of sedimentary environments. *Global Planet. Change* 137, 35–53.

Tanistrák J. 1969: Final geological report from the structural well Mojmírovce-1. *Open file report, Manuscript archive Nafta a.s. Plavecký Štvrtok*, 1–20 (in Slovak).

Vass D. 2002: Lithostratigraphy of Western Carpathians: Neogene and Buda Paleogene. *GÚDŠ*, Bratislava, 1–200.

Vozárová A., Jánošov J. & Šarinová K. 2003: Tourmaline-enriched horizons in the Lower Triassic quartzose sediments from Tribeč Mts., Tatric Unit, Western Carpathians (Slovakia). *Slovak Geological Magazine* 9, 1, 65–75.

Vozárová A. & Vozár J. 1988: Late Paleozoic in West Carpathians. *GÚDŠ*, 1–314.

Vrsaljko D. 1999: The Pannonian palaeoecology and biostratigraphy of Mollusca from Kostanjek-Medvednica Mt., Croatia. *Geologica Croatica* 52, 1, 9–27.

Whitney D.L. & Evans B.W. 2010: Abbreviations for names of rock-forming minerals. *Am. Mineral.* 95, 185–187.

Zahradníková B., Hudáčková N., Halásová E., Rybár S. & Kováč M. 2013: New findings from research of Sarmatian sediments from Ivanka-l well (Danube Basin, Slovakia). *Acta. Rer. Natur. Mus. Nat. Slov*. 59, 25–32.

Supplement

Suppl. 1. Key biostratigraphic data: foraminifera (F), nannofossils (N) and palynomorfs include dinoflagellata (P). U. Badenian=early Serravallian; Sarmatian=late Serravallian; Pannonian=Tortonian–Messinian; **a)** MOJ-1 well; **b)** IV-1 well; **c)** VR-1 well; **d)** ZM-1 well.

a) Mojmírovce 1 well (MOJ-1)

Depth (m)	Core	Discipline	Zone/Subzone	Event
848–854	8/1/15cm	P	Unassigned	Barren
848–854	8/1/ 75cm	P	Unassigned	Barren
848–854	8/2/50cm	F	Unassigned	Barren
		Other		Rhizoids
902–907	9/1/65cm	F	Unassigned	Barren
		Other		Fe oxides
955–960	10/2/ 90cm	F	Unassigned	Reworked: *Lenticulina* sp., *Globigerinella obesa*
		Other		Fe oxides, coal
955–960	10/3/75cm	F	Unassigned	Barren
		Other		?Crab excrements, coal, Fe oxides
955–960	10/3/95cm	F	Unassigned	Barren
		Other		Rhizoids
1000–1005	11/1/30cm	F	Unassigned	Barren
		Other		Ostracod shells–also articulated, coal
1253–1261	16/1/55cm	P	Unassigned	Barren
1253–1261	16/3/50cm	P	Unassigned	Barren
1253–1261	16/6	P	Unassigned	Barren
1253–1261	16/7/30cm	F	Unassigned	Barren
		Other		Gastropoda and Ostracoda fragments
1298–1303	17/1/25cm	F	Unassigned	Barren
		Other		Coal
1298–1303	17/2/40cm	F	Unassigned	Barren
		Other		
1298–1303	17/3/40cm	F	Unassigned	Barren
		Other		
1298–1303	17/5/30cm	F	Unassigned	Barren
		Other		Fe oxides
1351–1354	18/1–2/50	F	Unassigned	Barren
		Other		
1397–1401.5	19/1/60cm	F	Unassigned	Barren
		Other		Ostracoda fragments
1397–1401.5	19/3/25cm	P	Unassigned	Barren
1451–1455	20b/2/50	F	Unassigned	Barren
		P	Unassigned	Barren
		Other		Ostracoda fragments, fish bones
1500–1511	21/2–3/50	F	Unassigned	Barren
		Other		Coal
1500–1511	21/4–5	N	Unassigned	Barren
1795–1798	27/2–3/ 50	N	Unassigned	Barren
		F	Sarmatian	*Elphidium* sp.
1847–1851	28/1–2	F	Sarmatian	*Elphidium* sp., *E. josephinum, E. aculeatum, Ammonia parkinsoniana, Miliolidae*
1847–1851	28/3–4/50	F	Sarmatian	*Elphidium hauerinum, Aubignyna perlucida, Bolivina* spp., *Porosonion, Fissurina, Miliolidae*
		P	Unassigned	Phytoclasts, opaque
		Other		Coal rest, Fe oxides
1905–1910	29/2–4	F	Unassigned	Barren
		Other		Organic matter (algae)
2005–2010	31	N	Unassigned	Barren
		F	Unassigned	Barren
		Other		Dasycladacea *Halicoryne* aff. *morelleti*
2046–2051	32/4–5	F	Unassigned	Barren
		Other		Rhizoids
2095–2100	33/1–2/50	F	Late Badenian	*Bogdanowiczia pocutica* (*Bathysiphon pocutica*)

b) Ivanka 1 well (IV-1)

Depth (m)	Core	Discipline	Zone/Subzone	Event
1506–1509	3/2/ 65cm	F	Unassigned	Barren
		P	Pannonian	*Virgodinium asymmetricum, Spiniferites bentori pannonicus, Impagidinium spongianum*
1506–1509	3/3/ 50cm	F	Unassigned	Barren
		Other		Gastropoda and ostracoda fragments, fish bones
		P	Pannonian	*Achomosphaera* sp., *Spiniferites bentori pannonicus, Impagidinium spongianum, Pontiadinium pecsvaradensis*
1603–1612	5/3	N	Pannonian	*Reticulofenestra tegulata, Braarudosphaera bigelowii*, *B. bigelowii parvula* and allochthonous *Cyclicargolithus floridanus*, *Reticulofenestra bisecta*
		P	Pannonian	*Virgodinium asymmetricum, Spiniferites bentori pannonicus*
1758–1763	8/2/ 25cm	P	?Pannonian	*Virgodinium* sp., *Spiniferites* ssp., +*Spirogyra, Zygnema, Ovoidites*
1956–1961	12/3/50cm	F	Sarmatian	*Bolivina sarmatica, Bolivina* spp., *Porosonion* ex. gr. *granosum*
		Other		Fish bones
1956–1961	12/4/50cm	F		Barren
		Other		Organic matter, plant debris
1956–1961	12/5/50cm	F	Sarmatian	*Ammonia tepida, Bolivina* spp., *Nonion* spp., *Miliolidae,* reworked
		Other		Dasycladacea *Halicoryne* aff. *morelleti*
1956–1961	12/6/80cm	F	Unassigned	Barren
2010–2015	13/4/50cm	F	Unassigned	Barren
2040–2045	14/1/65cm	F	Sarmatian	*Nonion tumidulus, Miliolidae, Ammonia parkinsoniana, Elphidium* sp., *Streptochilus*
		Other		Acritarcha: *Pterospermella* sp., Dasycladacea *Halicoryne* aff. *morelleti,* pollen
2040–2045	14/2/45cm	F	Sarmatian	*Nubecularia crasraformis, Nonion* spp., *Bolivina* spp., *Miliolidae, Haynesina depressula, Elphidium* sp.
2090–2093	15/1/50cm	F	Sarmatian	*Ammonia tepida, Elphidium* sp., *Nonion* spp., *Miliolidae* reworked: *Cassigerinella globulosa, Haplophragmoides* sp.
		P	Unassigned	Barren redep. ?*Deflandrea* (paleogene dino)
		Other		Sponge spicules, Fe oxides, pyrite,
2090–2093	15/2/65cm	F	Unassigned	Barren
		P	Unassigned	Barren
		Other		Fish scales, coal, Fe oxides
2090–2093	15/3/30cm	F	? Sarmatian	*Porosonion* ex. gr. *granosum, Miliolidae*
		P	Unassigned	Barren
		Other		Organic matter
2158–2163	16/2/50cm	F	Unassigned	Barren
		Other		Organic matter
2158–2163	16/3/50cm	F	Unassigned	Barren
		Other		Organic matter
2274–2276	19/1/50cm	F	Unassigned	Barren
		Other		Mollusca fragments
2311–2316	20/31	N	Unassigned	*Braarudosphaera bigelowii, B. bigelowii parvula, Coccolithus pelagicus, Cyclicargolithus floridanus, Reticulofenestra bisecta, R. haqii, R. pseudoumbilicus, Sphenolithus moriformis* Eocene, Oligocene redeposits *Coccolithus formosus* and *Pontosphaera latelliptica*

c) Vráble 1 well (VR-1)

Depth (m)	Core	Discipline	Zone/Subzone	Event
603–607	3/3	P	Pannonian/ Tortonian/ NN9a-b	*Virgodinium asymmetricum, Pontiadinium pecsvaradensis*
703–707	5/1	P	Pannonian/ Tortonian/ NN9a-b	*Virgodinium asymmetricum, V. transformis, Pontiadinium pecsvaradensis, Impagidinium spongianum,*
750–755	6/1	P	Pannonian/ Tortonian/ NN9a-b	*Virgodinium asymmetricum, V. transformis, Impagidinium spongianum, Spiniferites bentori pannonicus, Spiniferites bentori oblongus, Achomosphaera* sp.
802–807	7/1	P	Pannonian/Tortonian/ NN9a-b	*Virgodinium asymmetricum, V. transformis, Spiniferites bentori pannonicus, Spiniferites bentori oblongus*
802–807	7/2	P	Pannonian/ Tortonian/ NN9a-b	*Virgodinium asymmetricum, V. transformis, Spiniferites bentori pannonicus, Spiniferites bentori oblongus, Pontiadinium pecsvaradensis, P. obesum + Spirogyra,* phytoclasts, -corr. S.b.oblongus Biochron 10.8 Ma (Magyar et al 1999), Central Paratethyan Spiniferites bentori oblongus zone (Suto-Szentai 1988) middle early Pannonian s.l.
802–807	7/4	P	Pannonian/Tortonian/ NN9a-b	*Spiniferites bentori pannonicus, Spiniferites bentori oblongus, Pontiadinium pecsvaradensis, P. obesum, V. transformis*
900–905	9/1/ 40cm	P	Pannonian/Tortonian/ NN9a-b	*Achomosphaera* sp., *Virgodinium asymmetricum, Pontiadinium pecsvaradensis, Spiniferites bentori pannonicus, Spiniferites bentori oblongus* -corr. S.b.oblongus Biochron 10.8 Ma (Magyar et al 1999), Central Paratethyan Spiniferites bentori oblongus zone (Suto-Szentai 1988) middle early Pannonian s.l.
950–955	10/1/ 50cm	P	?	Different palynofacies, more terrestrial and freshwater elements (*Zygnema*), aquatics (*Nuphar*), plus redepozited dinoflagellata (e.g. *Deflandrea*); no dinocyst
950–955	10/4/ 50cm	P	?	Small ungular organic remnants, no dinocyst
950–955	10/3	N	Unassigned	Poor sample, *Cyclicargolithus floridanus, Reticulofenestra pseudoumbilicus*
1000–1005	11/1/ 50cm	P	Pannonian	Dinoflagellata div.gen. et sp.
1103–1108	13/1/50cm	N	Pannonian	*Isolithus semenenko*, *Coccolithus miopelagicus*, *Cyclicargolithus floridanus*, *Calcidiscus*?, Ascidian spicules, *Reticulofenestra* sp.,
		F	Panonnian	*Milliammina fusca, M. subvelatina, Dogiellina* sp.
		Other		Fish remains, shark teeth
1103–1108	13/2/ 50cm	P	?	Dinoflagellata div.gen. et sp.
1103–1108	13/4	N	Unassigned	Barren
1149–1154	14/1/50cm	N	Pannonian	*Coccolithus pelagicus, C. miopelagicus*, *Cyclicargolithus floridanus*, *Calcidiscus tropicus*, *C. pataecus*, *Helicosphaera carteri, Rhabdosphaera* sp., *Umbilicosphaera rotula*, *Reticulofenestra pseudoumbilicus*, **Acme** *Isolithus semenenko,* reworking: *Coccolithus formosus, Microrhabdulus decoratus*
		F		*Dogielina* sp., poorly preserved *Miliammina ovata, M. subvelatina,* undeterminable agglutinated foraminifera
		Other		Fish teeth, Ostracoda shells
1149–1154	14/2/50cm	N	?Pannonian/ ?Sarmatian ?NN6	*Reticulofenestra pseudoumbilicus*, *Umbilicosphaera jafari*, ?*Isolithus semenenko,* **ABN** *Coccolithus pelagicus*, *Reticulofenestra haqii, Cyclicargolithus floridanus*, Paleogene reworking *Reticulofenestra bisecta*, *Pontosphaera latelliptica*, Cretaceous reworking
		F		Agglutinated foraminifera, *Dogielina* sp., *Miliammina velatina*, *M. subvelatina*
		P	?	Rare organic remnants
		Other		Ostracoda shells
1149–1154	14/3/50cm	N	?Pannonian/?Sarmatian ?NN6	*Coccolithus pelagicus*, *C. miopelagicus*, *Cyclicargolithus floridanus*, *Reticulofenestra haqii*, *Zygrhablithus bijugatus*, Paleogene and Cretaceous reworking
		F	Pannonian	?*Trochammina kibleri*, *Dogielina* sp.
		Other		Fish teet, Ostracoda shells, pyrite concretions strongly prevails
1203–1208	15/1/50cm	N	NN6 Sarmatian	*Coccolithus pelagicus, C. miopelagicus*, *Cyclicargolithus floridanus*, *Braarudosphaera bigelowii parvula, Calcidiscus tropicus*, C. *pataecus*?, *Discoaster deflandrei, R. pseudoumbilicus*, *Pontosphaera multipora*, *Sphenolithus abies*, Paleogene discoaster *D. lodoensis*, *Pontosphaera latelliptica*,
		F		*Ammonia tepida, Elphidium* sp., *Sinuloculina consobrina,* reworked Badenian foraminifera tests
		P	?	Well preserved pollen, no dinocyst
		Other		Carbonized floral rests, pyrite, fish bones, polens
1250–1255	16/1/50cm	N	NN6 Sarmatian	*Coccolithus pelagicus, Calcidiscus tropicus*, *C. macintyrei*?, *C. premacintyrei*, *C. pataecus*, *Pontosphaera latelliptica, Coccolithus miopelagicus, R. bisecta, Helicosphaera wallichii*
		F		2 specimens of Foraminifera tests *Elphidium* and *Ammonia*
		Other		Coal, organic linnigs, dasycladaceans, fish bones
1250–1255	16/2/50cm	N	Sarmatian	*Calcidiscus tropicus*, *C. pataecus*, *C. macintyrei*, *Braarudosphaera bigelowii parvula*
1250–1255	16/3/45cm	N	NN6 Sarmatian	*Calcidiscus tropicus*, *C. pataecus*, *C. leptoporus*, *Reticulofenestra pseudoumbilicus*, *Sphenolithus abies*
		F		Barren
		Other		Coal, fish bones
1250–1255	16/4/50cm	N	NN6 Sarmatian	*Coccolithus pelagicus, Calcidiscus, C. tropicus, C. pataecus*
		F		Barren
1250–1255	16/4	N	NN6 Sarmatian	*Coccolithus pelagicus, Calcidiscus, C. tropicus*,
1304–1309	17/1/20cm	N	Unassigned	Poor sample, *Coccolithus pelagicus*
		F		Autochtonnous can be test of *Ammonia* and *Cibicides boueanus*, Lower Miocene reworked foraminiferal tests as *Cassigerinella, Globigerina* sp. and *Nonion* sp.
		Other		Coal
1304–1309	17/5/20cm	N	NN 6 Sarmatian	*Coccolithus pelagicus*, *Helicosphaera carteri, Calcidiscus, C. tropicus, C. leptoporus, Sphenolithus abies, Reticulofenestra pseudoumbilicus*
		F		Autochtonnous can be tests of *Ammonia* Miocene reworked foraminiferal tests of big diameters as *Cassigerinella, Globigerina* sp. and *Nonion* sp

c) Vráble 1 well (VR-1) (continued)

Depth (m)	Core	Discipline	Zone/Subzone	Event
1350–1355	18/2/50cm	N	NN6 Sarmatian	*Coccolithus pelagicus*, *Calcidiscus tropicus*, *C. macintyrei*, *C. leptoporus*?, *C. patecus*?, *Rhabdosphaera* sp., *Reticulofenestra pseudoumbilicus*, *Sphenolithus abies*, *Braarudosphaera bigelowii bigelowii*, *Pontosphaera latelliptica, Prediscosphaera cretacea*
		F	Sarmatian	*Ammonia tepida* macrospheric, *Elphidium macellum, E. josephinum, E. hauerinum*
		Other		Pyrite, Ca concretions, fish bones, coal
1350–1355	18/3/50cm	N	Unassigned	Barren
		F	Sarmatian	*Elphidium josephinum, Ammonia tepida, Porosinonion* ex. gr. *granosum,* rare Badenian redeposites
		Other		Ca and Fe concretions, fish scales
1350–1355	18/4/50cm	N	Unassigned	Barren
		F	Unassigned	Barren
		Other		Coal
1405–1409	19/1/50cm	N	Unassigned	Barren
		F	Unassigned	Barren
1405–1409	19/2/25cm	N	Unassigned	Barren
		F	Sarmatian	Autochtonnous *Nonion biporus*, O/M redeposites
		other		Pyritized valves of diatomace
1405–1409	19/2/80cm	N	NN6 Sarmatian	**Acme** *Calcidiscus, C. tropicus+Coccolithus pelagicus*
		F	Unassigned	Barren
1405–1409	19/4/45cm	N	NN6 Sarmatian	*Coccolithus formosus, Calcidiscus tropicus, C. premacintyrei, C. pataecus, C. leptoporus*? *Discoaster variabilis*?*, Lanternithus minutus*
		F	Unassigned	Barren
		Other		Coal
1405–1409	19/5/50cm	N	NN6 Sarmatian	*Coccolithus pelagicus, Calcidiscus tropicus, C. premacintyrei*
		F	Unassigned	Small tests of foraminifera, probably all reworked *Globigerina* sp. div., *Bulimina elongata*
		Other		Organic matter
1450–1455	20/2/10cm	N	Unassigned	Barren
		F	Unassigned	Very bad preserved miliolidae foraminiferal tests
		Other		Coal
1450–1455	20/3/10cm	N	Unassigned	Barren
		F	Unassigned	*Porosonion granosum, Ammonia parkinsoniana, Elphidium macellum*
		Other		Organic matter
1450–1455	20/4/50cm	N	Unassigned	Barren
		F		Barren
		Other		Organic matter
1450–1455	20/5/50cm	N	Unassigned	Barren
		F		*Nonion* sp. indet
		Other		Coal, organic matter, dasycladacea *Halicornia* sp.
1450–1455	20/8/50cm	N	Unassigned	Barren
		F	Unassigned	Very rare reworked planktic foraminiferal tests as *Globigerinita uvula*
1505–1510	21/2/50cm	N	NN6 Sarmatian	**Acme** *Calcidiscus, C. tropicus+C. pataecus*?
		F	Unassigned	*Elphidium macellum,* reworked globigerinids
		Other		Coal
1505–1510	21/3/50cm	N	NN6 Sarmatian	**Acme** *Calcidiscus, C. tropicus, C. leptoporus, Reticulofenestra pseudoumbilicus*, *R. haqii, Reticulofenestra* sp., *Braarudosphaera bigelowii parvula, Coccolithus pelagicus*, Paleogene, *C. formosus*
		F	Sarmatian	*Cycloforina badenensis, Ammonia tepida, Elphidium josephinum, E. macellum, Porosononion granosum,* reworked planktic foraminiferal tests
		Other		Coal, sponge spines
1505–1510	21/4/50cm	N	NN6 Sarmatian	**Acme** *Calcidiscus, C. tropicus*, *Reticulofenestra pseudoumbilicus*, *Coccolithus pelagicus*
		F		Massive portion of reworked ?Upper Badenian foraminiferal benthos
		Other		Fe crusts, organic matter
1550–1555	22/1/50cm	N	Unassigned	Poor sample, *Coccolithus pelagicus,* lots of organic matter
1550–1555	22/2/50cm	N	Unassigned	Poor sample, *Coccolithus pelagicus, Cyclicargolithus floridanus, Reticulofenestra haqii, R. pseudoumbilicus,* lots of organic matter
		F		*Ammoniana tepida, Nonion* sp., *Globigerina* sp.
		Other		Organic matter, ostracods, porifera spines, dasycladacea *Halicoryne* aff. *morelleti*
1550–1555	22/3/50cm	N	Unassigned	Poor sample, *Coccolithus pelagicus,* lots of organic matter
		F	Sarmatian	*Ammonia tepida*, *Nonion* sp.
		Other		*Halicornnia* sp.
1550–1555	22/4/50cm	N	Unassigned	Poor sample, *Reticulofenestra bisecta,* lots of organic matter, pyrite
		F		?*Streptochilus* sp., *Cibicides boueanus, Ammonia tepida, Cycloforina badenensis, Porosononion granosum*
		Other		Coal
1652–1657	24/2/50cm	N	NN6 Sarmatian	*Calcidiscus* **acme***, Calcidiscus tropicus, C. leptoporus/pataecus*?*, Coccolithus pelagicus, Cyclicargolithus floridanus*
		F	Unassigned	Barren
		Other		Organic matter
1652–1657	24/3/50cm	N	NN6 Sarmatian	*Calcidiscus tropicus* small *Calcidiscus*, *Sphenolinithus abies*?, *Umbilicosphaera rotula, U. jafari*
		F	Unassigned	Barren
		Other		Poriferan spikes
1700–1705	25/1/50cm	N	Unassigned	Poor sample, *Coccolithus pelagicus, Reticulofenestra bisecta*
		F	Unassigned	Barren

c) Vráble 1 well (VR-1) (continued)

Depth (m)	**Core**	**Discipline**	**Zone/Subzone**	**Event**
1745–1750	26/1/50cm	N	NN 6 Sarmatian	*Calcidiscus leptoporus/pataecus*?, *Holodiscolithus macroporus*, *Reticulofenestra pseudoumbilicus, Braarudosphaera bigelowii bigelowii, Braarudosphaera bigelowii parvula, Pontosphaera japonica,* reworked *Lanternithus minutus, Zygrhablithus bijugatus, Coccolithus formosus,* pyrite
1745–1750	26/2/50cm	N	NN 6 ?Sarmatian	*Reticulofenestra pseudoumbilicus, Holodiscolithus macroporus*, *Calcidiscus leptoporus,* **ABN** *Coccolithus pelagicus, Reticulofenestra haqii, Cyclicargolithus floridanus*
		F		Milliolidae foraminifers visible in lumps, very tinny, may be dissolved
		Other		Dasycladacea *Halicornia* sp.
1745–1750	26/4/50cm	N	NN6 Sarmatian	*Braarudosphaera bigelowii parvula*, *Holodiscolithus macroporus*, *Reticulofenestra pseudoumbilicus, Calcidiscus tropicus*, *C. leptoporus, C. pataecus*?, *Helicosphaera walbersdorfensis, Umbilicosphaera rotula*
		F	Unassigned	Barren
		Other		Coal
1745–1750	26/5/50cm	N	NN6 ?Sarmatian	*Braarudosphaera bigelowii bigelowii*, *Calcidiscus pataecus*?, *C. tropicus*, *Holodiscolithus macroporus*, *Reticulofenestra pseudoumbilicus,* **ABN** *Coccolithus pelagicus, Reticulofenestra haqii*
		F	Sarmatian	**Acme** *Anomalinoides badenensis*, reworked *Globigerinoides* sp.
		Other		Pyritized diatomace
1801–1804	27/1/50cm	N	?Badenian	*Braarudosphaera bigelowii bigelowii*, *B. bigelowii parvula, Calcidiscus* sp., *Helicosphaera wallichii*?, *H. walbersdorfensis, Reticulofenestra pseudoumbilicus,* **ABN** *Coccolithus pelagicus, Reticulofenestra haqii, Cyclicargolithus floridanus, Coronocyclus nitescens, Spenolithus heteromorphus* Paleogene reworking nannofossils: *Reticulofenestra hillae, Cyclicargolithus abisectus, Pontosphaera latelliptica, Helicosphaera recta*, *Lanternithus minutus, Zygrhablithus bijugatus, R. bisecta, R. stavensis, Tribrachiatus orthostylus;* Cretaceous reworking nannofossils: *Micula staurophora, Arkhangelskiella cymbiformis*
		F		Small foraminifera shells, ? Reworked?
		P	Badenian/ Sarmatian	?*Cleistosphaeridinium placacanthum* (or reworked)
		Other		Autigene pyrite, coal, seeds, organic matter, poriferan spikes
2054–2059	32/2A	N	Unassigned	Barren
2202–2207	35/3/90cm	N	Unassigned	Barren

d) Zlaté Moravce 1 well (ZM-1)

Depth (m.)	Core	Discipline	Zone/Subzone	Event
551–556	2/2	P	Pannonian	*Impagidinium spongianum, Spirogyra*
551–556	2/4	P	Pannonian	*Impagidinium spongianum, Spirogyra*
599–604	3/3	P	Pannonian	*Impagidinium spongianum, Spiniferites bentori pannonicus*
653–658	4/1	P	Pannonian	*Spiniferites bentori pannonicus*
954–959	10/1/50cm	N	Unassigned	Barren/?*Thoracosphaera* fragment
		F	Unassigned	Barren
1005–1010	11/3,4/50 cm	N	Pannonian	**ABN** *Reticulofenestra tegulata* and *Pontosphaera japonica*, *Reticulofenestra pseudoumbilicus*, *R. haqii*, *R. minuta*, *Coccolithus pelagicus*, *Cyclicargolithus floridanus*
		F	Unassigned	Barren
1046–1051	12/2/50	F		**Acme** *Bolivina dilatata maxima, Bulimina elongata,* cassidulinids (reworked)
1046–1051	12/4	N	NN6 Sarmatian	*Calcidiscus* spp., *C. leptoporus*, *Umbilicosphaera jafari*
1099–1104	13/4/50cm	F	Unassigned	Barren
1145–1150	14/1	N	Unassigned	Barren
1201–1206	15/2	N	NN6 ?Late Badenian ?Sarmatian	*Helicosphaera walbersdorfensis*, *H. wallichii*, *H. carteri*, *Sphenolithus abies*, *Reticulofenestra pseudoumbilicus*, *Calcidiscus premacintyrei*, *C. macintyrei*, *C. tropicus*, *C. leptoporus*, *Umbilicosphaera rotula*, *Holodiscolithus macroporus*, *Braarudosphaera bigelowii bigelowii*, *Rhabdosphaera* sp., **ABN** *Coccolithus pelagicus*, *Reticulofenestra haqii*
1253–1258	16/2/50cm	F		Extremely rich and diversified assemblage dominated by *Bolivina dilatata maxima*, *Melonis pompilioides*, *Angulogerina angulosa, Valvulineria complanata*
		Other		Bryozoans, ostracoda valves
1253–1258	16/3	N	NN6 Late Badenian	*Sphenolithus abies, Braarudosphaera bigelowii parvula, Reticulofenestra pseudoumbilicus*, *Umbilicosphaera jafari*, *Holodiscolithus macroporus*, **ABN** *Coccolithus pelagicus*, *Reticulofenestra haqii*, reworked *Coccolithus formosus, Arkhangelskiella cymbiformis*
1346–1351	18/2/50cm	N	NN6 ?Badenian ?Sarmatian	*Calcidiscus premacintyrei*, C. *tropicus*, *Coccolithus pelagicus, Reticulofenestra haqii, Cyclicargolithus floridanus, Sphenolithus abies, Umbilicosphaera jafari, Reticulofenestra stavensis*
		F	Upper Badenian	Fragments of agglutinated foraminifers, *Nonion communis, Bulimina elongata, Uvigerina semiornata*
		P	Corr.with NN6/BulBol	*Melitasphaeridium choanophorum*
1346–1351	18/3/50cm	N	Unassigned	Barren
		F		*Spirorutilus carinatus, Haplophragmoides wilsoni, Reticulophragmium, Bathysiphon* sp.
		P	Corr.with NN6/BulBol	*Cleistosphaeridinium placacanthum*
1346–1351	18/4/50cm	F		Dominated by *Haplophragmoides wilsoni, Reticulophragmium, Ammobaculites, Bathysiphon* sp.
		P	Unassigned	Phytoclasts, opaque
1346–1351	18/5/50cm	N	Unassigned	Barren
		F		Agglutinated types of foraminifers dominated by *Haplophragmoides wilsoni, Reticulophragmium, Ammobaculites, Bathysiphon* sp.
1405–1410	19/1/50cm	N	Unassigned	Barren
		F	Unassigned	Possible agglutinated foraminifera or testaceans, *Ammobaculites*
		Other		Organic matter, *Glyptostrobus* seeds and cones
1405–1410	19/2/50cm	N	Unassigned	Barren
		F		Undetermined agglutinated foraminifera or testaceans
1494–1499	21/1/50cm	N	Unassigned	Barren
		P	Unassigned	Barren
		F	Unassigned	Barren
1494–1499	21/2	N	Unassigned	Barren
1494–1499	21/3/50cm	N	Unassigned	Barren
		P	Unassigned	Barren
		F	Unassigned	Barren
1494–1499	21/4/50cm	N	Unassigned	Barren
		F	Unassigned	Barren
1494–1499	21/5	N	Unassigned	Barren
1553–1558	22/1/50cm	N	Unassigned	Barren/?*Thoracosphaera*, ?*Reticulofenestra* sp.
		F	Unassigned	Barren
1708–1711	25/1/50cm	N	Unassigned	Barren
		F	Unassigned	Barren

Suppl. 2. Complete fauna and flora list: **a)** Dasycladacean algae; **b)** Foraminifera; **c)** Nannofossils; **d)** Palynomorfs.

a) Dasycladacean algae

Halicoryne aff. *morelleti* (Pokorný, 1948)

b) Foraminifera

Angulogerina angulosa (Williamson, 1858)
Anomalinoides dividens Łuczkowska, 1967
Bathysiphon Sars, 1872 sp.
Bogdanowiczia pocutica Pishvanova, 1967
Bolivina dilatata maxima (Cicha & Zapletalová, 1963)
Bolivina sarmatica Didkowski, 1959
Bulimina elongata d'Orbigny, 1826
Cassigerinella globulosa Egger, 1857
Chiloguembelina cubensis (Palmer, 1934)
Dogielina Bogdanovich & Voloshinova, 1949 sp.
Elphidium aculeatum (d'Orbigny, 1846)
Elphidium hauerinum (d'Orbigny, 1846)
Elphidium josephinum (d'Orbigny, 1846)
Globigerina concinna Reuss, 1850
Globigerinella obesa (Bolli, 1957)
Haplophragmoides Cushman, 1910 sp.
Haplophragmoides wilsoni Smith, 1948
Melonis pompilioides (Fichtel & Moll, 1798)
Miliammina Heron-Allen & Earland, 1930
Miliammina fusca (Brady, 1870)
Miliammina subvelatina Venglinsky, 1975
Miliammina velatina Venglinsky, 1961
*Nonion communis (*d'Orbigny, 1846)
Porosononion granosum (d'Orbigny, 1846)
Quinqueloculina badenensis = Cycloforina badenensis (d'Orbigny, 1846)
Reticulophragmium Maync, 1955
Spirorutilus carinatus (d'Orbigny, 1846)
Trilobatus trilobus (Reuss, 1850)
?*Trochammina kibleri* Venglinsky, 1961
Uvigerina semiornata d'Orbigny, 1846
Valvulineria complanata (d'Orbigny, 1846)

c) Nannofossils

Arkhangelskiella cymbiformis Vekshina, 1959
Braarudosphaera bigelowii (Gran & Braarud, 1935) Deflandre, 1947
Braarudosphaera bigelowii parvula Stradner, 1960
Calcidiscus Kamptner, 1950
Calcidiscus leptoporus (Murray & Blackman, 1898) Loeblich & Tappan, 1978
Calcidiscus macintyrei (Bukry & Bramlette, 1969) Loeblich & Tappan, 1978
Calcidiscus pataecus (Gartner, 1967) de Kaenel & Villa, 1996
Calcidiscus premacintyrei Theodoridis, 1984
Calcidiscus tropicus (Kamptner, 1955) Varol, 1989 *sensu* Gartner, 1992
Coccolithus formosus (Kamptner, 1963) Wise, 1973
Coccolithus miopelagicus Bukry, 1971
Coccolithus pelagicus (Wallich, 1877) Schiller, 1930
Coronocyclus nitescens (Kamptner, 1963) Bramlette & Wilcoxon, 1967
Cyclicargolithus abisectus (Muller, 1970) Wise, 1973
Cyclicargolithus floridanus (Roth & Hay, in Hay et al., 1967) Bukry, 1971
Discoaster deflandrei Bramlette & Riedel, 1954
Discoaster lodoensis Bramlette & Riedel, 1954
Discoaster variabilis Martini & Bramlette, 1963
Helicosphaera carteri (Wallich, 1877) Kamptner, 1954
Helicosphaera recta (Haq, 1966) Jafar & Martini, 1975
Helicosphaera walbersdorfensis Muller, 1974
Helicosphaera wallichii (Lohmann, 1902) Okada & McIntyre, 1977
Holodiscolithus macroporus (Deflandre, in Deflandre & Fert, 1954) Roth, 1970
Isolithus semenenko Luljeva, 1989
Lanternithus minutus Stradner, 1962
Microrhabdulus decoratus Deflandre, 1959
Micula staurophora (Gardet, 1955) Stradner, 1963
Pontosphaera japonica (Takayama, 1967) Nishida, 1971
Pontosphaera latelliptica (Báldi-Beke, in Báldi-Beke & Báldi, 1974) Perch-Nielsen, 1984
Pontosphaera multipora (Kamptner, 1948 ex Deflandre in Deflandre & Fert, 1954) Roth, 1970)
Prediscosphaera cretacea (Arkhangelsky, 1912) Gartner, 1968
Reticulofenestra Hay, Mohler & Wade, 1966
Reticulofenestra bisecta (Hay, Mohler & Wade, 1966) Roth, 1970
Reticulofenestra haqii Backman, 1978
Reticulofenestra hillae Bukry & Percival, 1971
Reticulofenestra minuta Roth, 1970
Reticulofenestra pseudoumbilicus (Gartner, 1967) Gartner, 1969
Reticulofenestra stavensis (Levin & Joerger, 1967) Varol, 1989
Reticulofenestra tegulata (Bóna & Gál, 1985; Ćorić & Gross, 2004)
Rhabdosphaera Haeckel, 1894
Sphenolithus abies Deflandre in Deflandre & Fert, 1954
Sphenolithus heteromorphus Deflandre, 1953
Sphenolithus moriformis (Bronnimann & Stradner, 1960) Bramlette & Wilcoxon, 1967
Thoracosphaera Kamptner, 1927
Tribrachiatus orthostylus Shamrai, 1963
Umbilicosphaera jafari Muller, 1974
Umbilicosphaera rotula (Kamptner, 1956) Varol, 1982
Zygrhablithus bijugatus (Deflandre in Deflandre & Fert, 1954) Deflandre, 1959

d) Palynomorfs

Achomosphaera Evitt, 1963
Cleistosphaeridinium placacanthum Deflandre & Cookson, 1955
Deflandrea Eisenack, 1938
Impagidinium spongianum Sütő-Szentai, 1985
Melitasphaeridium choanophorum (Deflandre & Cookson, 1955) Harland & Hill, 1979
Pontiadinium obesum Sütő-Szentai, 1982
Pontiadinium pecsvaradensis Sütő-Szentai, 1982*
Spiniferites Mantell, 1850
Spiniferites bentori (Rossignol, 1964) Wall & Dale, 1970 ssp. *oblongus* Sütő-Szentai, 1986
Spiniferites bentori (Rossignol, 1964) Wall & Dale, 1970 ssp. *pannonicus* Sütő-Szentai, 1986
Virgodinium Sütő-Szentai, 2010
Virgodinium asymmetricum Sütő-Szentai, 2010
Virgodinium transformis Sütő-Szentai, 2010

* Despite the Lentin and Williams index (2017 edition) with redefined genus to ?*Impagidinium*, we used in whole manuscript the species name *Pontiadinium pecsvaradensis* (=?*pecsvaradense*) according the Sütő-Szentai´s and Bakrac´s publications to be able to correlate biozones.